Lamont-Doherty Earth Observatory of Columbia University

Abstract

We have analyzed the spatial and temporal variability of chlorophyll in the Atlantic Ocean off the Portugal coast using satellite imagery from 1979 to 1986 in conjunction with wind data. The spatial patterns in the imagery show the typical inshore-offshore and east-west gradients, while the temporal patterns show seasonal high winter values and low summer values. In the satellite imagery for the period 1979–1986, stable meso- and large-scale patterns recurred despite interannual differences in absolute satellite-derived pigment concentration.

Introduction

Understanding the relationships between the biological and physical regimes has long been a basic goal in biological oceanography. How does the physical regime influence the phytoplankton abundances found at a given time and place? "Plant" abundance patterns must in principle differ from those of passive drifters because of birth and death rates of phytoplankton, including grazing by zooplankton, which affect those patterns, as do physical stirring, mixing and sinking. Significant changes in physical forcing usually produce measurable changes in phytoplankton distribution, but the changes are often poorly understood and unpredictable.

An important purpose of satellite remote sensing is the detection of large-scale changes in the ocean and atmosphere both in space and time. Most of the ship-based measurements are limited primarily to smaller spatial scales and shorter temporal scales. The Coastal Zone Color Scanner (CZCS) flown on the Nimbus-7 satellite supplied the scientific community with a densely sampled, biological time series of pigment concentration over large areas.

We used a complete seven-year time series of ocean-color imagery around Portugal from 1979 to 1986 from the Coastal Zone Color Scanner for exploring (a) seasonality and interannual variation of the continental shelf; (b) the meso- and large-scale spatial structure of the pigment patterns; and (c) correlation between wind data and upwelling pigment events.

Data and Methods

Wind Data

The geostrophic winds for the four selected regions along the Atlantic coastline of Spain and Portugal were made available by Dr. Smith of NOAA (La Jolla). These regions, made of rectangles 3-degrees to a side, are centered on <45°N, 8.5°W>, <42°N, 10°W>, <39°N, 10°W>, and <36°N, 7.5°W> and are named boxes 3, 4, 5 and 6 (Figure 1). The format of the data was an 8-character date (year month date hour) and columns in pairs of north-south and east-west components for each of the regions. The positive values are winds to the north and to the east in tenths of meters per second. Each data set is made up of 6 hourly observations between January 1967 and December 1986. Statistical summaries of the region were done using the Statgraf statistical program. Both frequency spectrum and periodogram statistical procedures were used to analyze this data. Frequency spectrum allows for the decomposition of the variance of the data into contributions over a range of frequencies. The periodogram utilizes the fast Fourier Transform procedure and plots the squared amplitudes of sinusoids. The periodogram is scaled such that if the mean of the series is zero, the sum of the periodogram ordinates will be equal the sum of the squared data values. The integrated periodogram procedure verifies whether the data points in a time series are random.

Satellite Data

We have used the NASA regional (4km resolution) data sets consisting of daily and monthly images. At U.R.I. the CZCS images were selected and corrected for geometric distortion. The center of the images is 40° north latitude and 10.5 ° west longitude (Figure 2). Six hundred and sixty-five images were examined to pick the clearest 60 images, one per month.

Four areas (boxes) in the image where selected for future analyses. The location of these boxes was coincident with our wind data above. The error in the x and y location was within 1 to 3 pixels because "ringing" effects were avoided (*i.e.*, a pixel is corrupted as the scanner moves from a bright target to a dark target like clouds). Statistical summaries of the region were done using the Statgraf statistical program . Seasonality in each location (boxes 3 to 6) was further investigated with periodogram and by integrated periodogram describing the cycle/sampling interval (see wind section). The correlation function of Statgraf, computes correlation coefficients for a time series and lagged values of the same vector. The function plots vertical bars for lags from one to the maximum lag specified.

Results

Wind Data

Daily and monthly means of wind data were computed for each of the four regions. Our findings are as follows:

(1) Trends are found in the wind data. The upwelling winds from April to September increase in intensity over the period 1967-1986 (Figure 3). This trend is very evident in location 6 (Gibralter) and in location 7 (Morocco). Location 4 and 5 (Portugal) decreasein intensity from the beginning of the 80's with a reverse trend occurring between 1983-1984;
(2) Seasonality was estimated by integrating periodograms of the monthly means. The seasonality is estimated and given in proportion to the total variance over 1967-1986. A high fraction of the variance (over 50%) which is seasonal is found in locations 4, 5 and 6 (Figures 4 and 5);

(3) Interannual variability is larger than seasonal variability (Figures 6, 7 and 8). Location 5 presents the largest difference between maximum and minimum wind speed.

Satellite Data

The seven-year time series of images from July 1979 to December 1985 showed considerable variability of satellite-derived pigments in both time and space. Values of pigment concentration ranged from 0.05 to 8.00 mg chl-m^{-3} in the study area.

Although satellite imagery was available intermittently during the seven years studied, the four areas averaged over the Portugal coast showed similar temporal trends. These trends are (a) seasonality with low biomass values in the summer, and peak values in the winter; (b) interannual variations greater than seasonal variations; and (c) upwelling events in the west coast. A time series of the four locations is shown in Figures 9, 10, 11 and 12 . This time series show typical spikes in derived chlorophyll pigments, and so it is difficult to detect any seasonality or interannual variation (Figures 13, 14, 15 and 16). On the other hand, the seasonal averaged plots of the four locations (boxes 3 to 6) show seasonality and interannual variation. The monthly averaged plots show north-south and inshore-offshore gradients, with higher values on the west coast and inshore. Location 3, in the north, shows a low biomass with strong seasonality. Locations 4 and 5, on the west coast of Portugal, had high biomass values with large interannual variation (evident in location 4 as the upwelling season). And location 6, in the south, presented the lowest biomass and smallest seasonality (Figures 13, 14, 15 and 16). Seasonality for each area (boxes 3 to 6) was estimated by integrating periodograms of the monthly means (Figures 17, 18, 19 and 20). The seasonality is estimated and given in proportion to the total variance over 1978-1986. A high fraction of the variance (over 50%) which is seasonal is found in box 3 (Figure 17).

Estimated cross-correlations between the four areas of satellite pigment were computed (box 3 vs box 4 etc, Figures 21 to 31). As anticipated, boxes 4 and 5 are correlated.

The winter season (December-February) appeared remarkably similar throughout the coast for the seven year period. We saw an annually constant offshore-inshore gradient, and a narrow coastal band of concentrated pigment.

In the spring months (March-June), a wide band of higher pigment waters was further offshore. A strong eddy exchange between the Mediterranean Sea and the Atlantic Ocean was seen during this period as well.

The summer months (July-August) had two steep gradients, an offshore-west and a north-south. The former was steeper, with high pigment structures (jets, filaments, eddies) stretching offshore; and the later was less intense in structure and pigment gradient. Reduced or increased upwelling during these years is difficult to determine given the coverage and small number of images available for the summer months.

The autumn months (September-November) showed a straight longitudinal boundary, less convoluted and farther offshore, that results in an offshore-inshore gradient and an increase in pigment content of the waters reaching far offshore. The high-pigment structure in the study area generally was overlying bathymetry features.

Interannual cycling of large patterns was seen as a complex structure in spring, with eddies, meanders, and jets, decayed to a progressively homogeneous condition in the winter, which then repeated the previous spring's patterns.

Correlation of Satellite Pigment with Wind Data

Estimated cross-correlations between satellite pigment with wind data were computed for each location (north-south and east-west component, Figures 32 to 39). Cross-correlation of satellite pigment with wind data was not coincident with upwelling events.

Discussion

Based on the data included in this study, the temporal and spatial upwelling structures (ie, eddies, jets and filaments) off the coast of Portugal are very similar to that seen off the coast of California. But the conclusions that can be drawn from this study are limited by the fact that it involves no sea-true data. Future studies should include, and be correlated with, ship hydrographic data.

The satellite data included in this study is limited by a number of variables. These include meteorological conditions (cloud coverage, barometric fluctuations) and mechanical conditions (retrieval problems, degradation of the sensor). The variability of cloudiness had three effects. First, it influenced directly the availability of clear images, and may have affected indirectly the phytoplankton through variations of solar irradiance. Second, the available clear images are not evenly spaced in time, and important information on same phases of the annual cycle is missing. Poor atmospheric conditions can make a visible-light sensor (CZCS) useless until the atmosphere clears. Third, atmospheric variability in time and space results in defective atmospheric correction, for instance, during periods of winds from the land or during very clear conditions, because a uniform set of atmospheric parameters was used for producing the Global data set. The available images will be for a single phase of the annual cycle and results may then be biased toward these meteorological conditions. Therefore, meteorological conditions have serious implications for satellite oceanography off the Portugal coast by affecting both the availability of images and the different confidence levels for the pigment value derived from the CZCS.

Figure Captions

Figure 1. Regional map with box positions used for estimating wind speed.

Figure 2. Satellite study area.

Figure 3. Six-month (April-September) averages of daily estimates of alongshore wind stress (NS i.e., the negative values are winds to the south in tenth of meters per second). The locations are indicated in Figure 1. Data has been filtred by a simple moving average of 2 months.

Figures 4 & 5. The relative importance of seasonality in the variability of wind speed (monthly averages 1967-87). The curve is the integrated value of variability from the long-term to the short-term (0.083 cycles = 1/2 season). The central line represents "white" noise or variability evenly distributed in frequency; lines parallel to the center line represents 75% and 95% limits of white noise given the number of observations in the time series.

Figures 6, 7 & 8. The interannual variability of wind data by region. The horizontal line represents the monthly average (according to the time series), while the vertical lines represents the successive annual estimates of wind speed cubed for each month. In figure 6 the time series is from 1967 to 1987, while in figures 7 and 8, is from 1978 to 1986.

Figures 9, 10, 11 & 12. Time series of satellite pigments data (1978-1986) for the four regions (box 3 to 6).

Figures 13, 14, 15 & 16. The interannual variability of satellite pigments data by region. The horizontal line represents the monthly average (1978-1986), while the vertical lines represents the successive annual estimates of wind speed cubed for each month.

Figures 17, 18, 19 & 20. The relative importance of seasonality in the variability of satellite pigment data (monthly averages 1978-1986). The curve is the integrated value of variability from the long-term to the short-term (0.083 cycles = 1/2 season). The central line represents the "white" noise or variability evenly distributed in frequency; lines parallel to the center line represents 75% and 95% limits of white noise given the number of observations in the time series.

Figures 21 to 31. Cross correlations between satellite pigment regions (i.e., box 3 vs box 4, etc.).

Figures 32 to 39. Cross correlation between satellite pigment regions and wind area.

Regions (1-9)
NS1-9
EW1-9

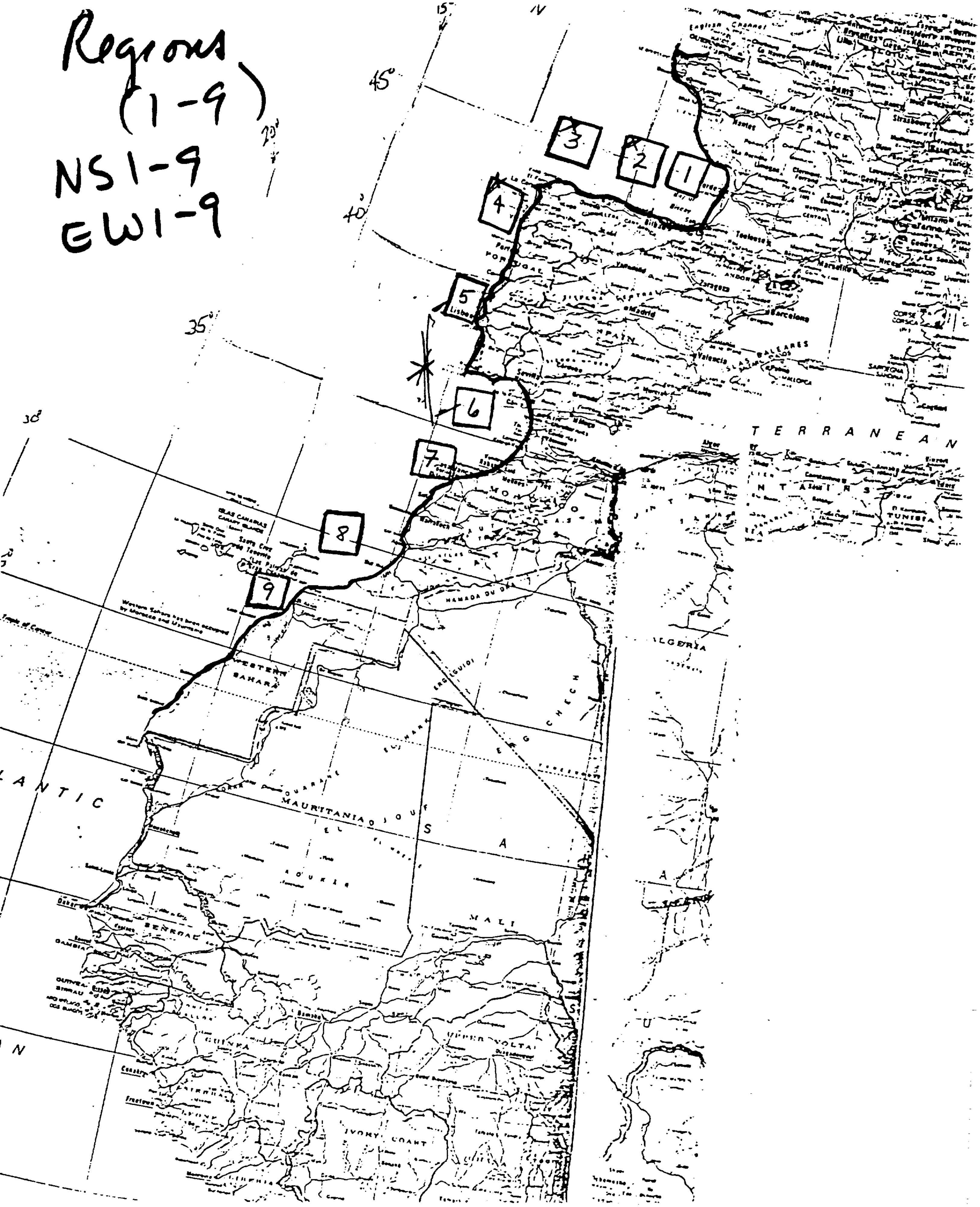

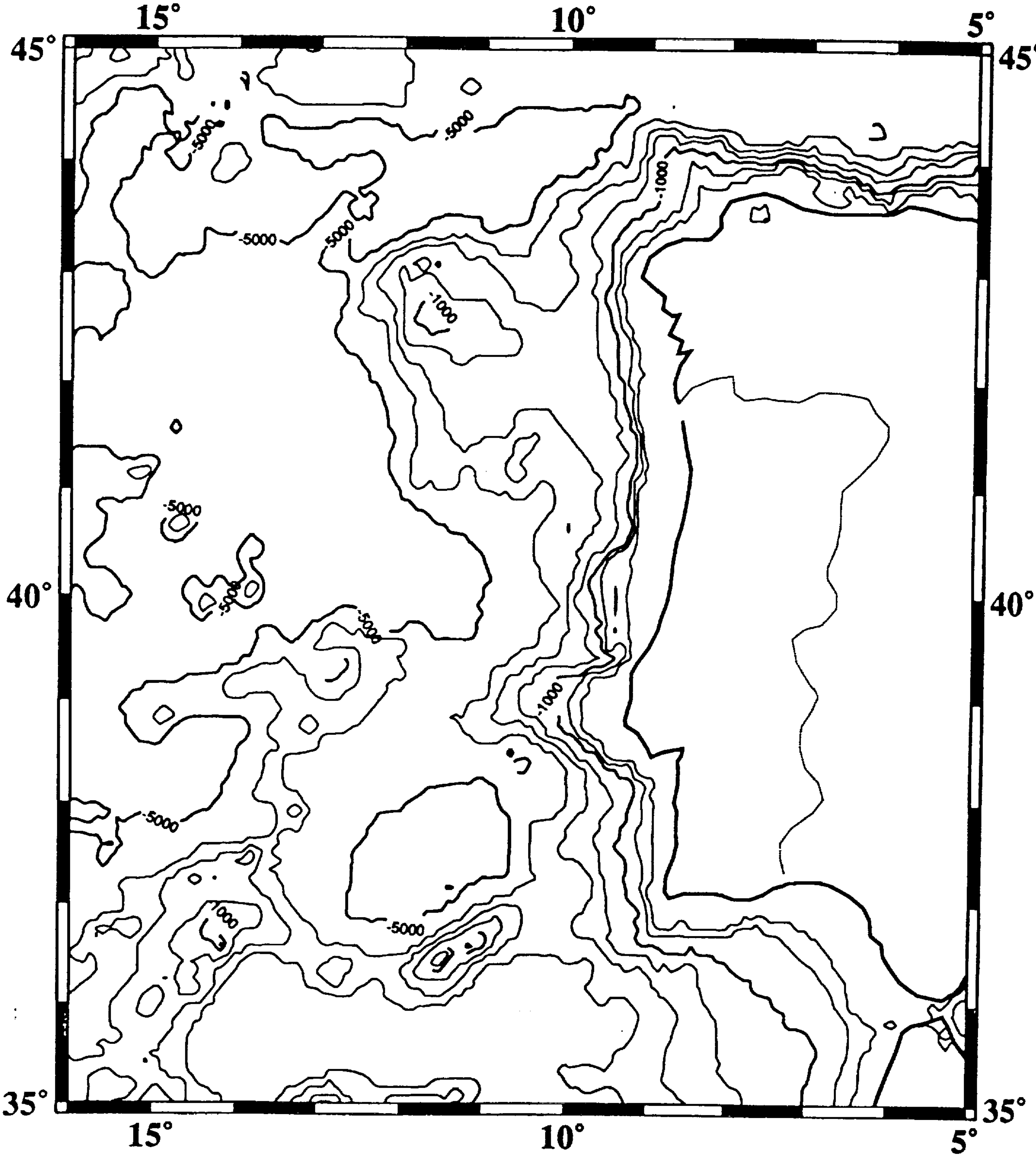

15°
10°
5°
45°
45°
40°
40°
35°
35°
15°
10°
5°
-5000
-5000
-5000
-5000
-1000
-1000
-5000
-5000
-5000
-1000
-5000
-1000
-5000

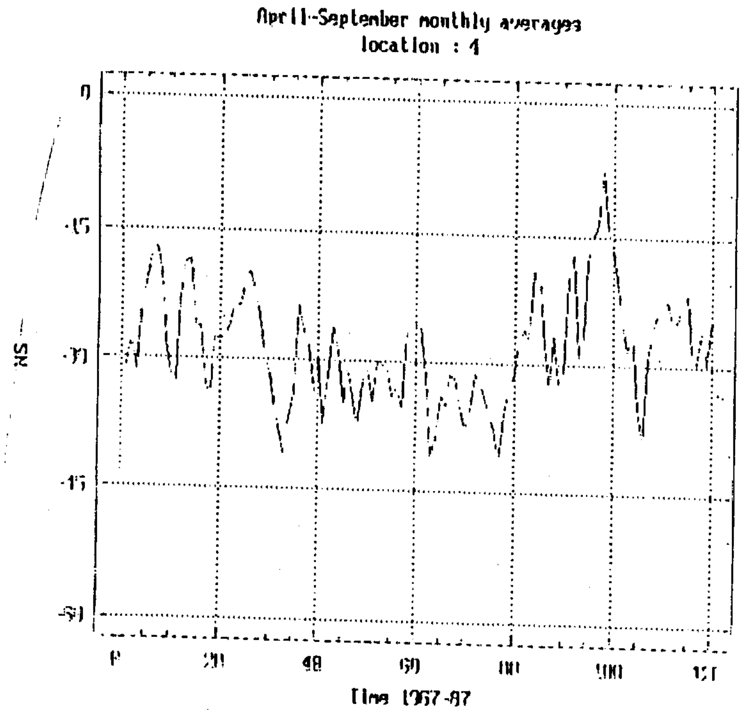
April-September monthly averages
location : 4
SN
time 1967-87

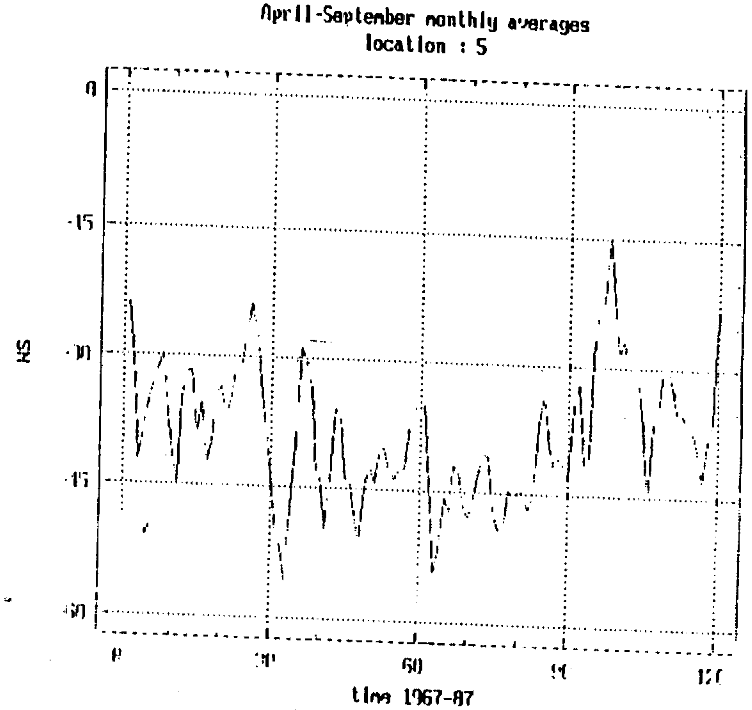
April-September monthly averages
location : 5
SN
time 1967-87

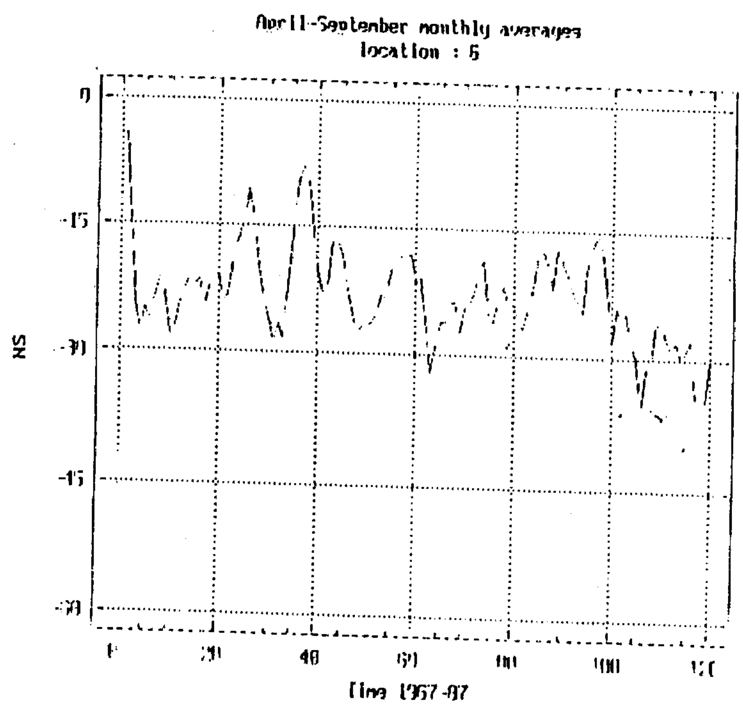
April-September monthly averages
location : 6
SN
time 1967-87

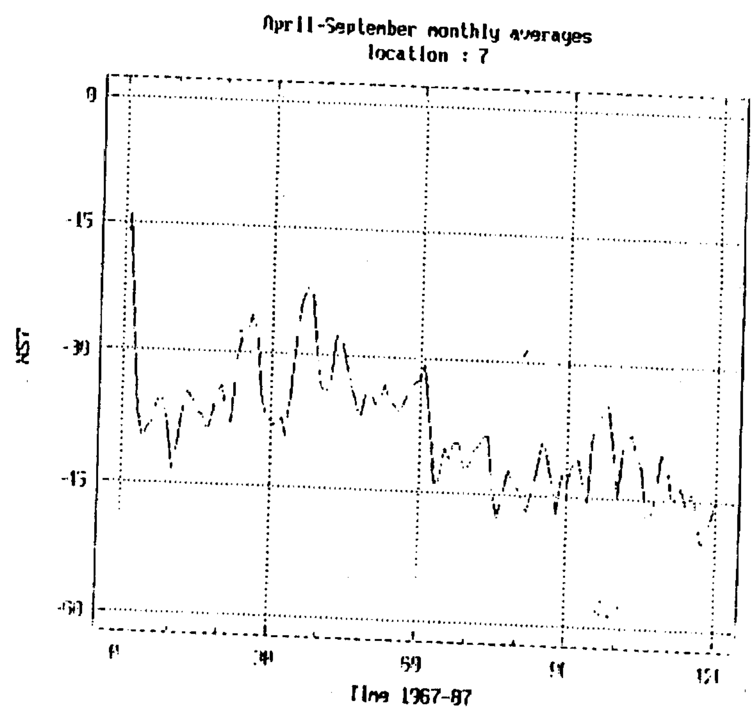
April-September monthly averages
location : 7
NST
time 1967-87

Integrated periodogram for NS3.output

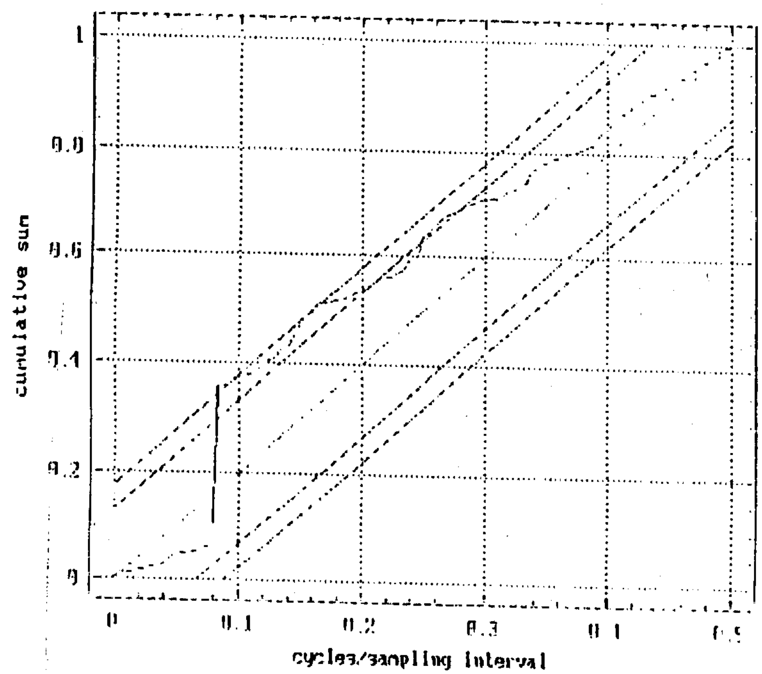

Integrated periodogram for EW3.output

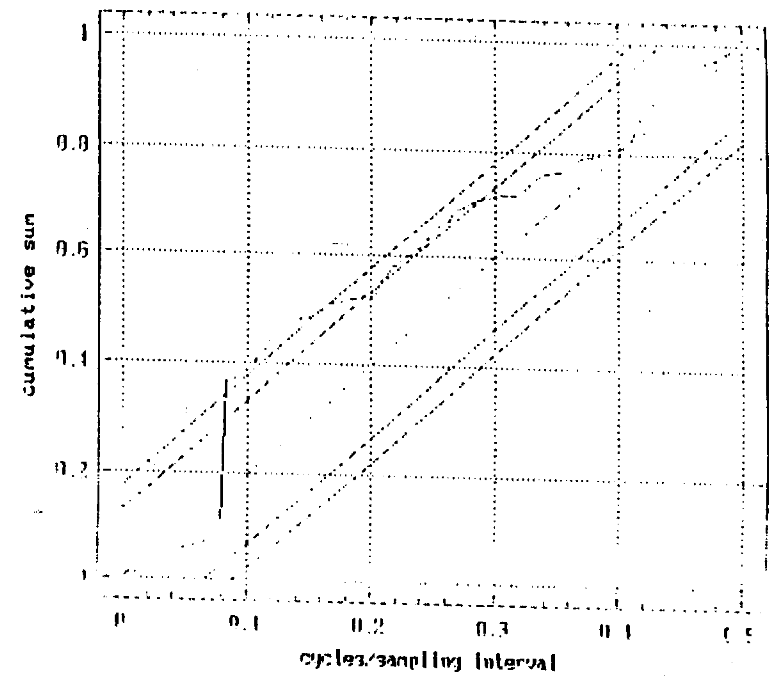

Integrated periodogram for NS4.output

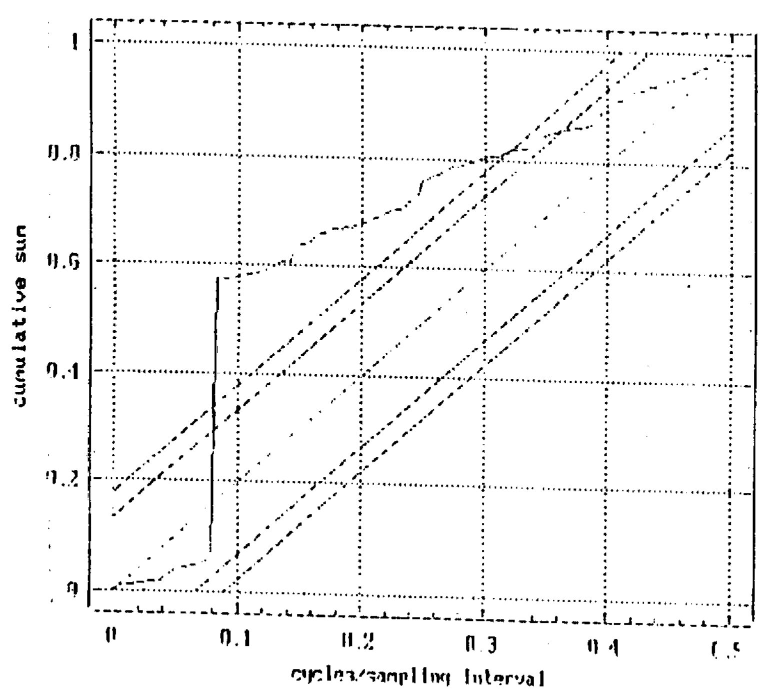

Integrated periodogram for EW4.output

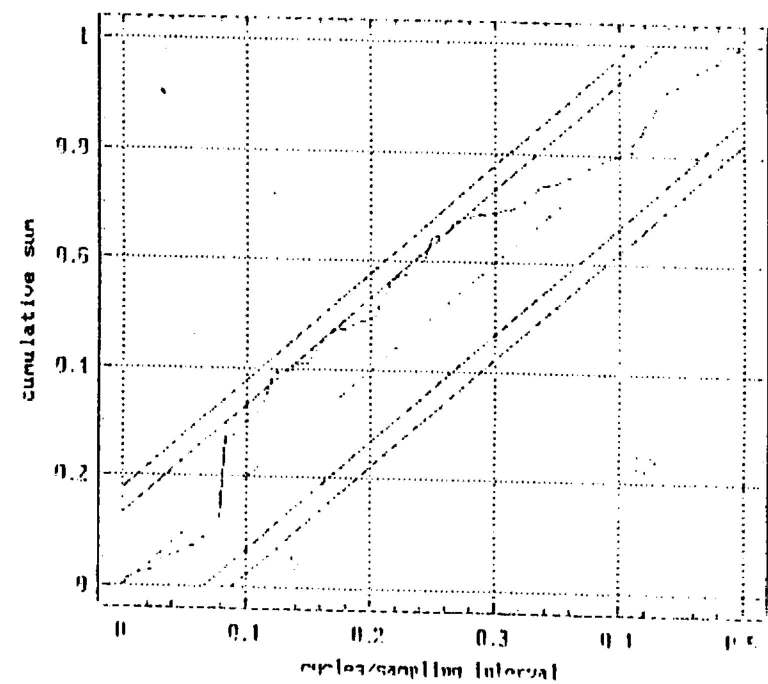

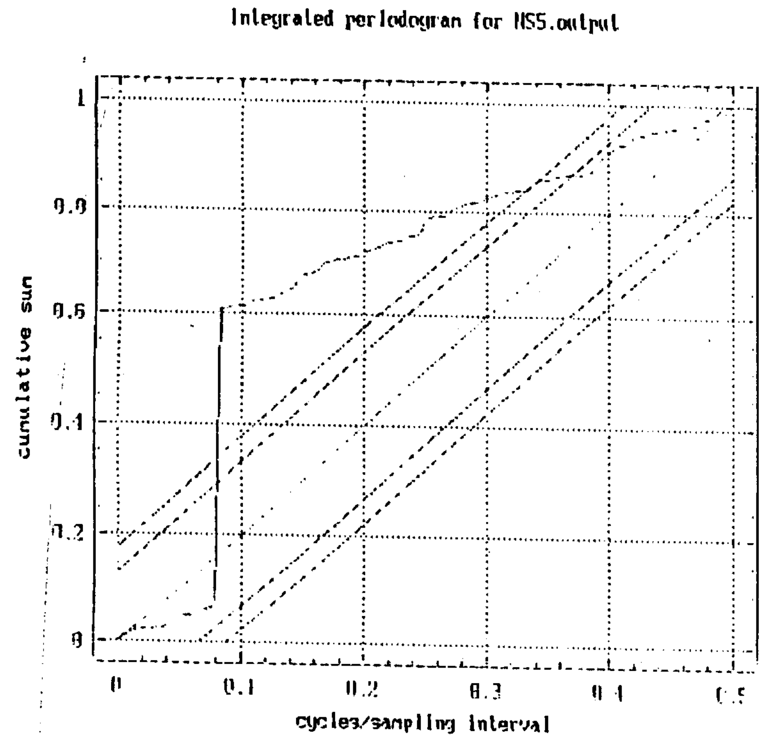
Integrated periodogram for NS5.output
cumulative sum
cycles/sampling interval

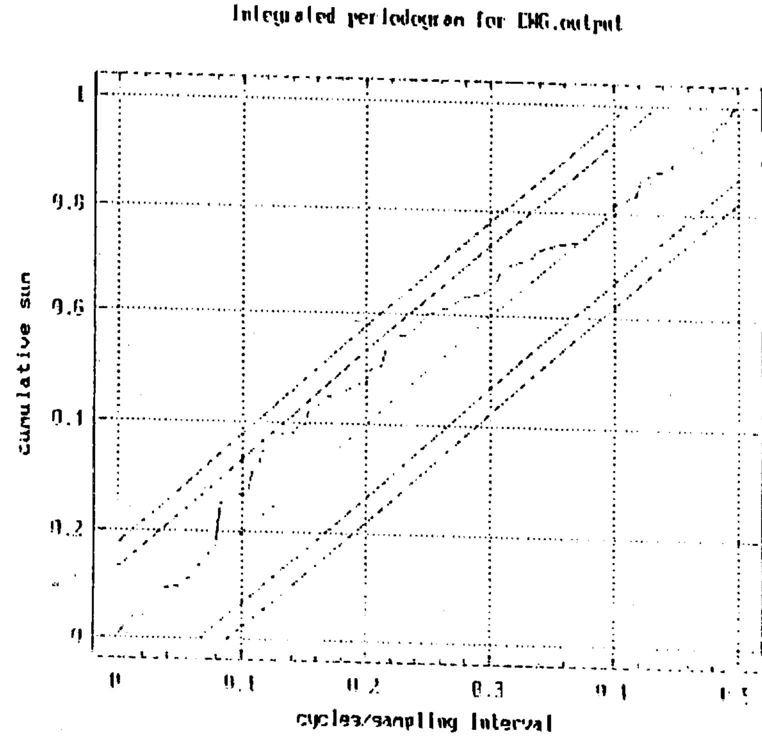
Integrated periodogram for EW6.output
cumulative sum
cycles/sampling interval

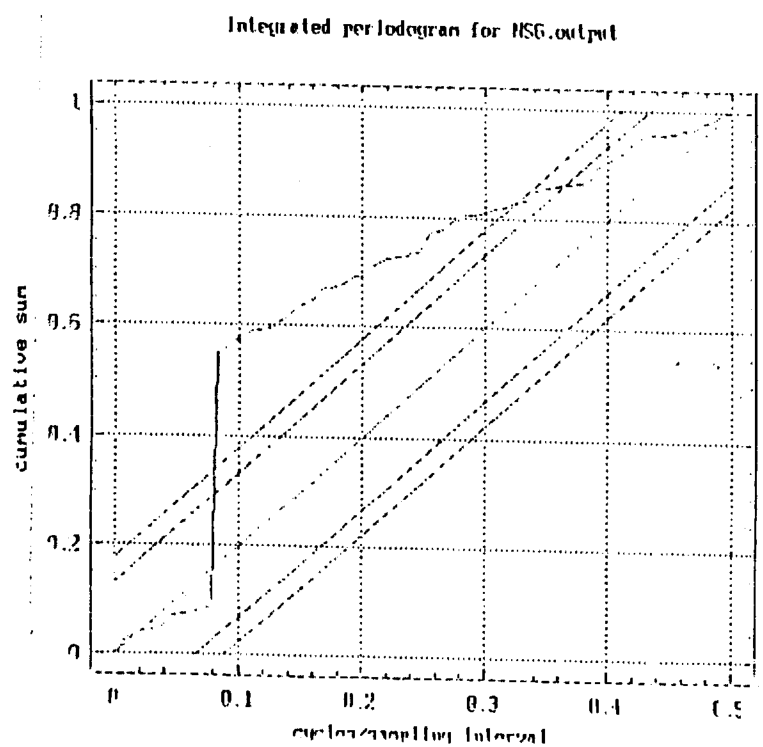
Integrated periodogram for NS6.output
cumulative sum

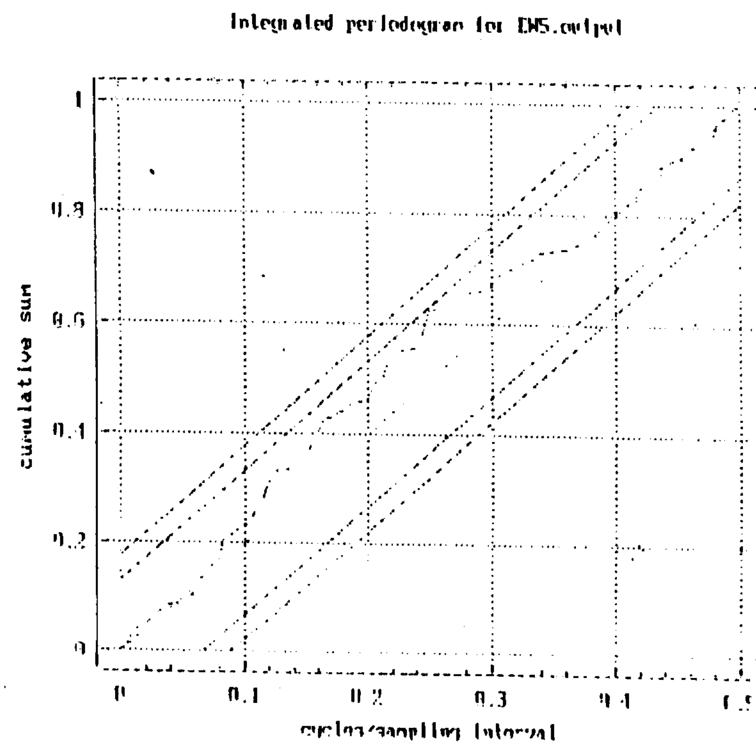
Integrated periodogram for EW5.output
cumulative sum

WINDS 1967-07: location 3

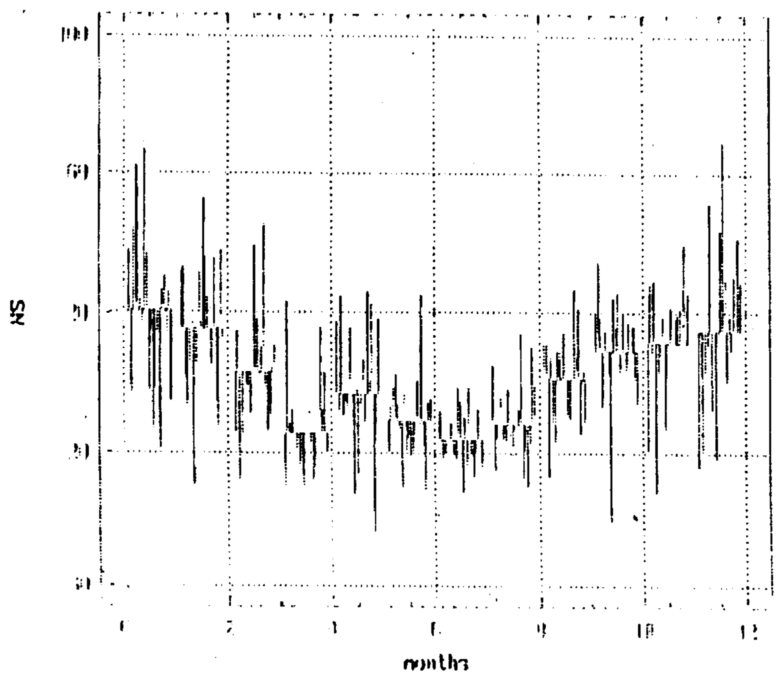

WINDS 1967-07: location 4

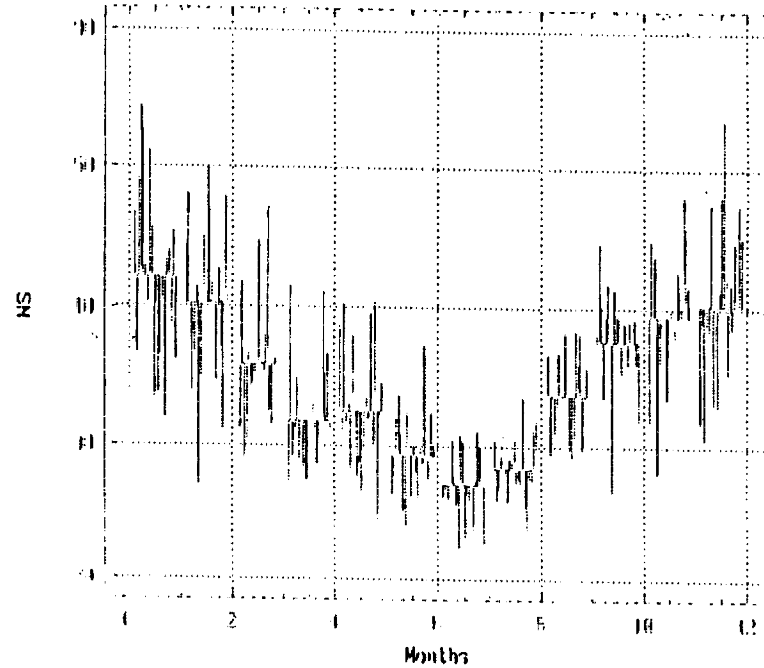

WINDS 1967-07: location 5

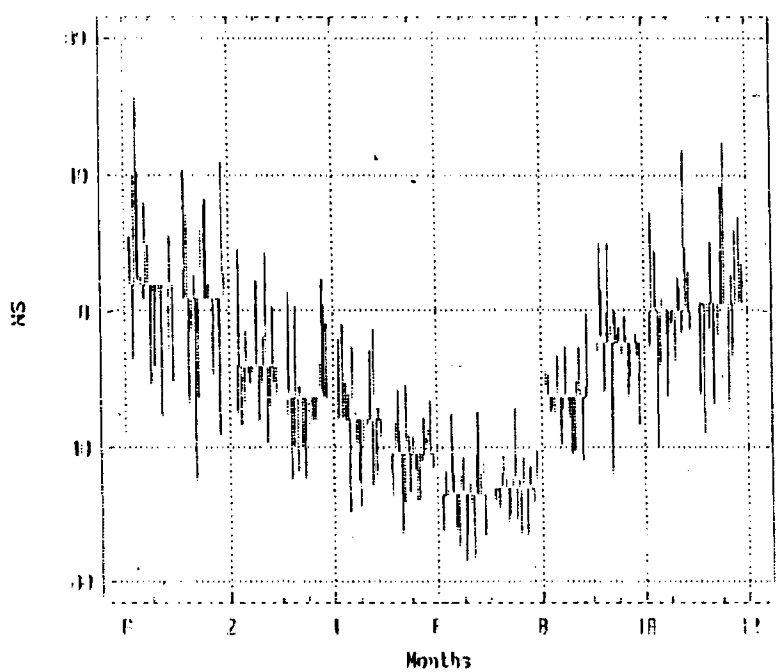

WINDS 1967-07: location 6

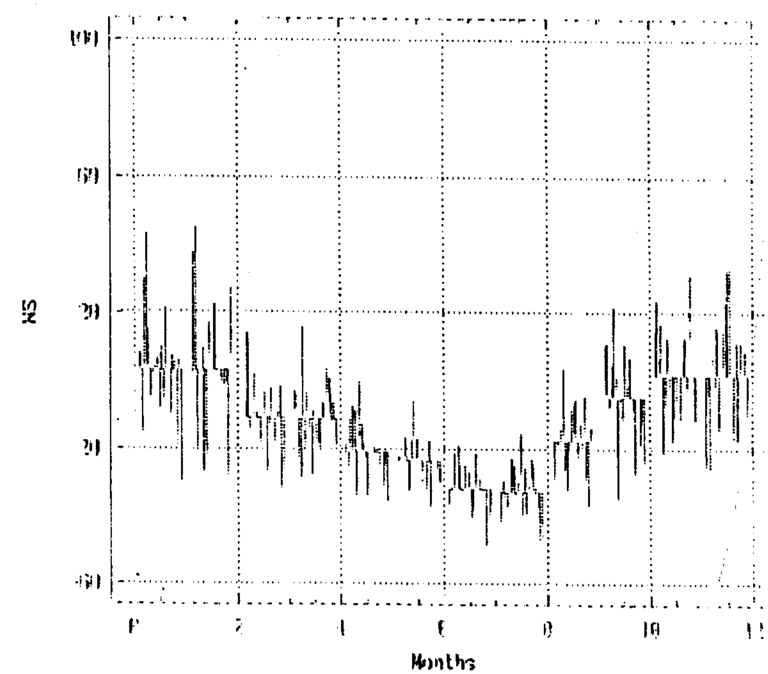

WINDS 1979-86 : location 3

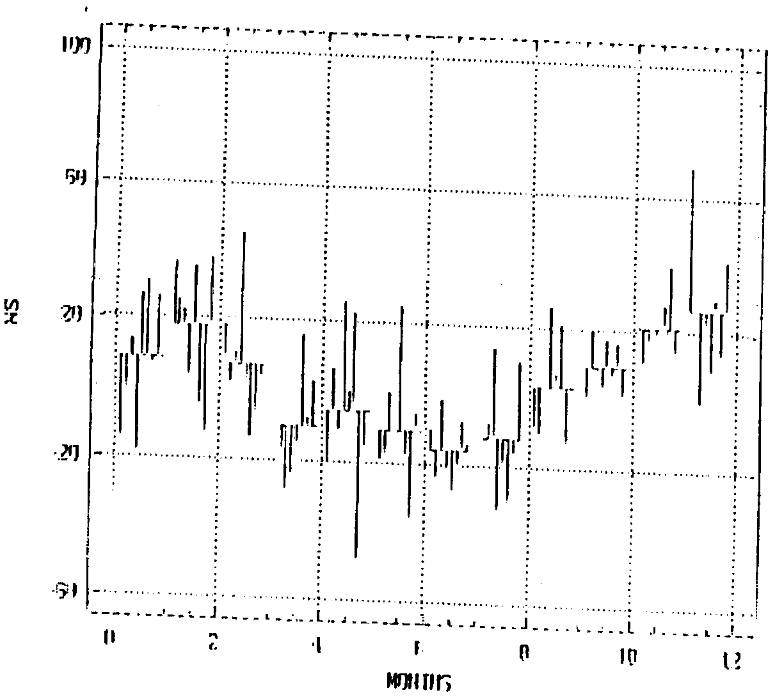

WINDS 1979-86: location 3

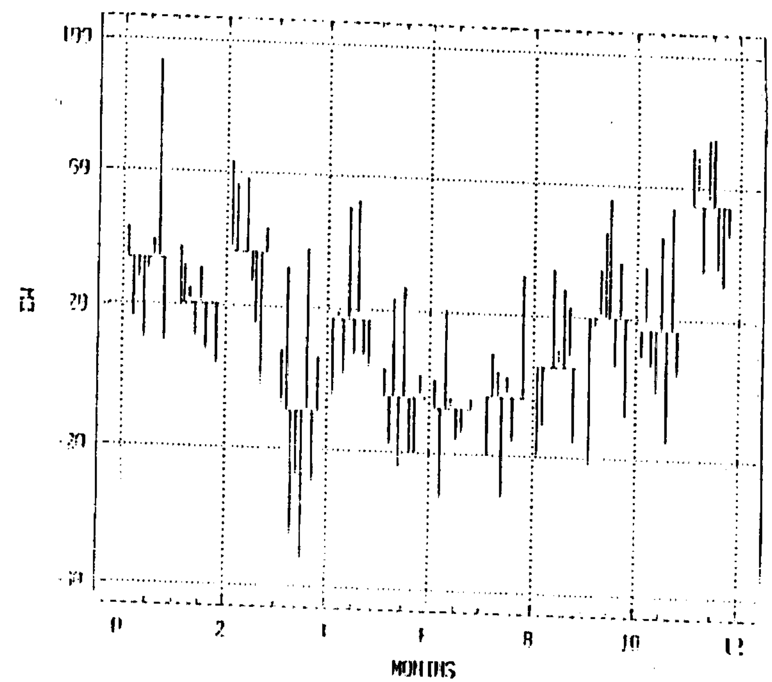

WINDS 1979-86: location 4

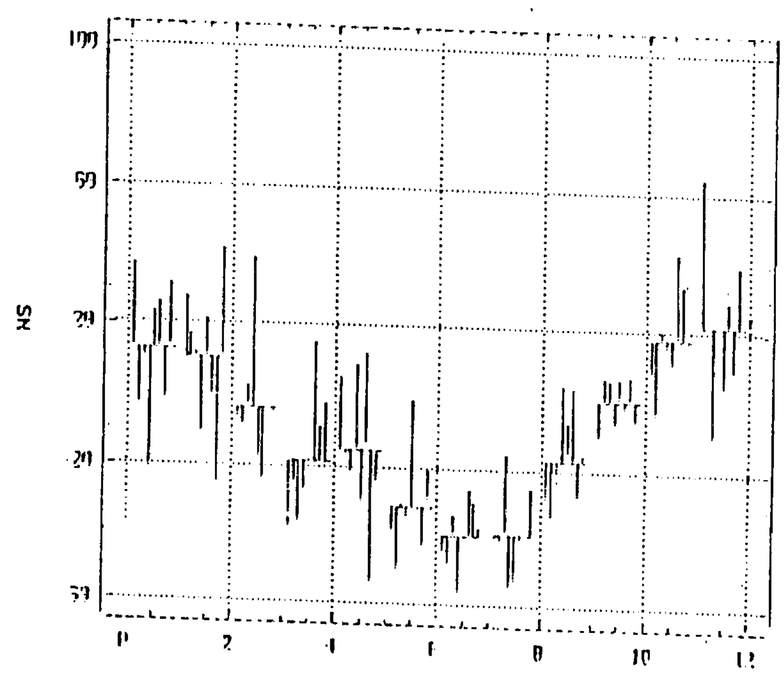

WINDS 1979-86: location 4

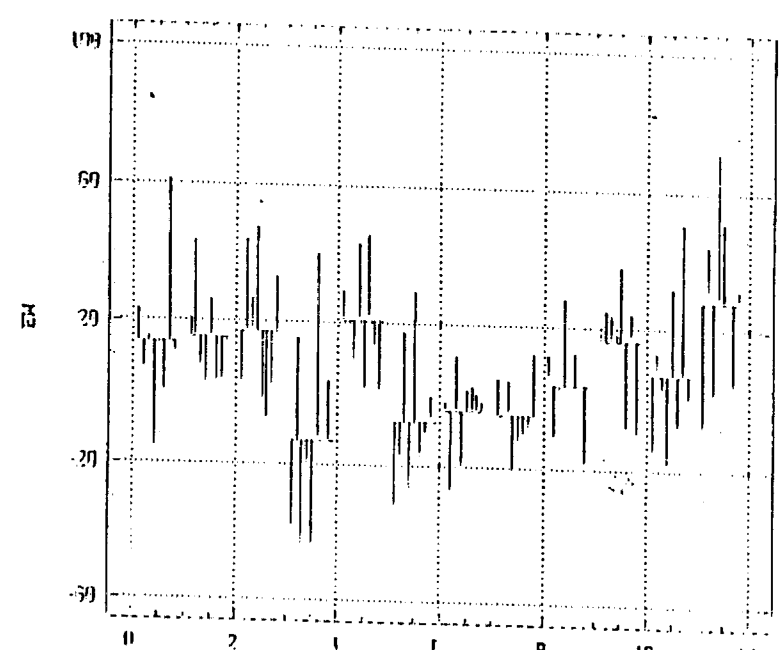

WINDS 1979-06: location 5

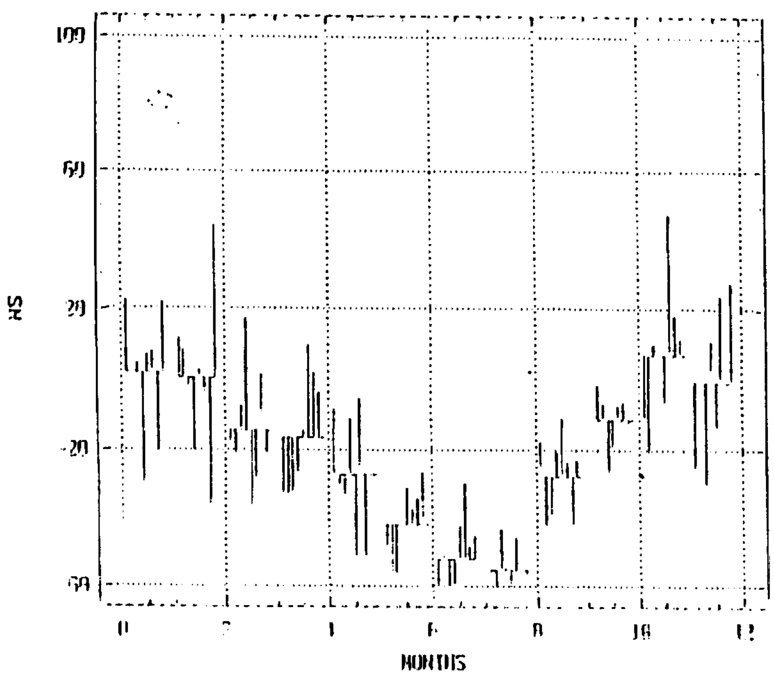

WINDS 1979-06: location 5

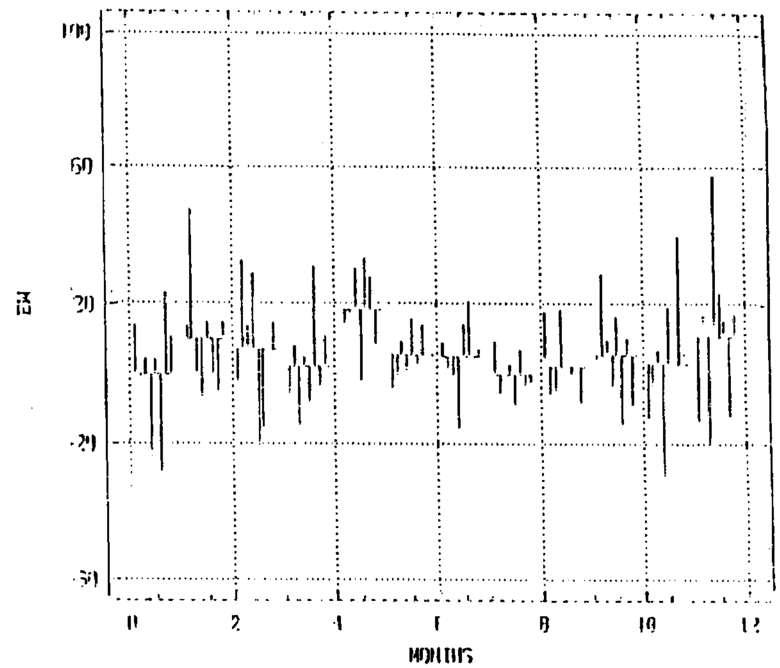

WINDS 1979-06: location 6

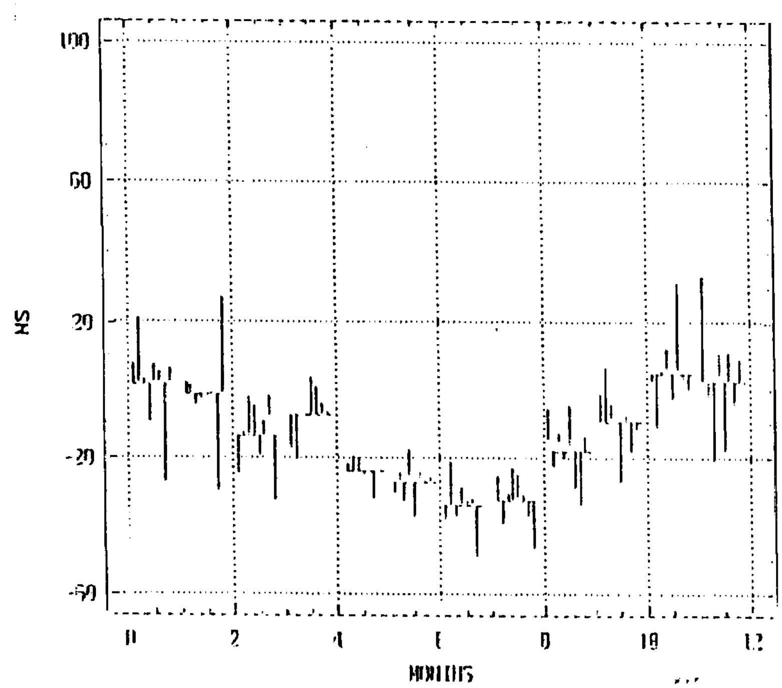

WINDS 1979-06: location 6

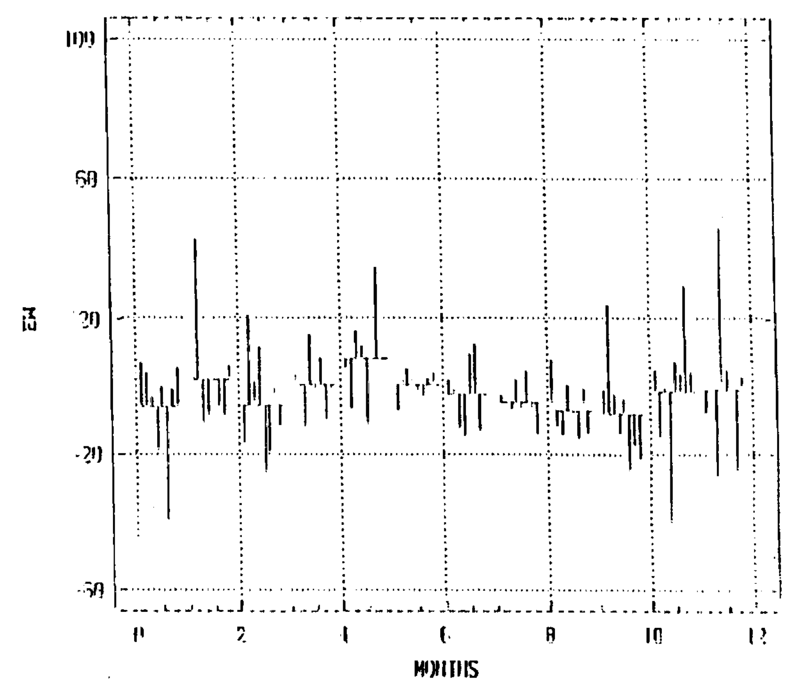

ORIGINAL PAGE IS
OF POOR QUALITY

Time Sequence Plot

Box 3

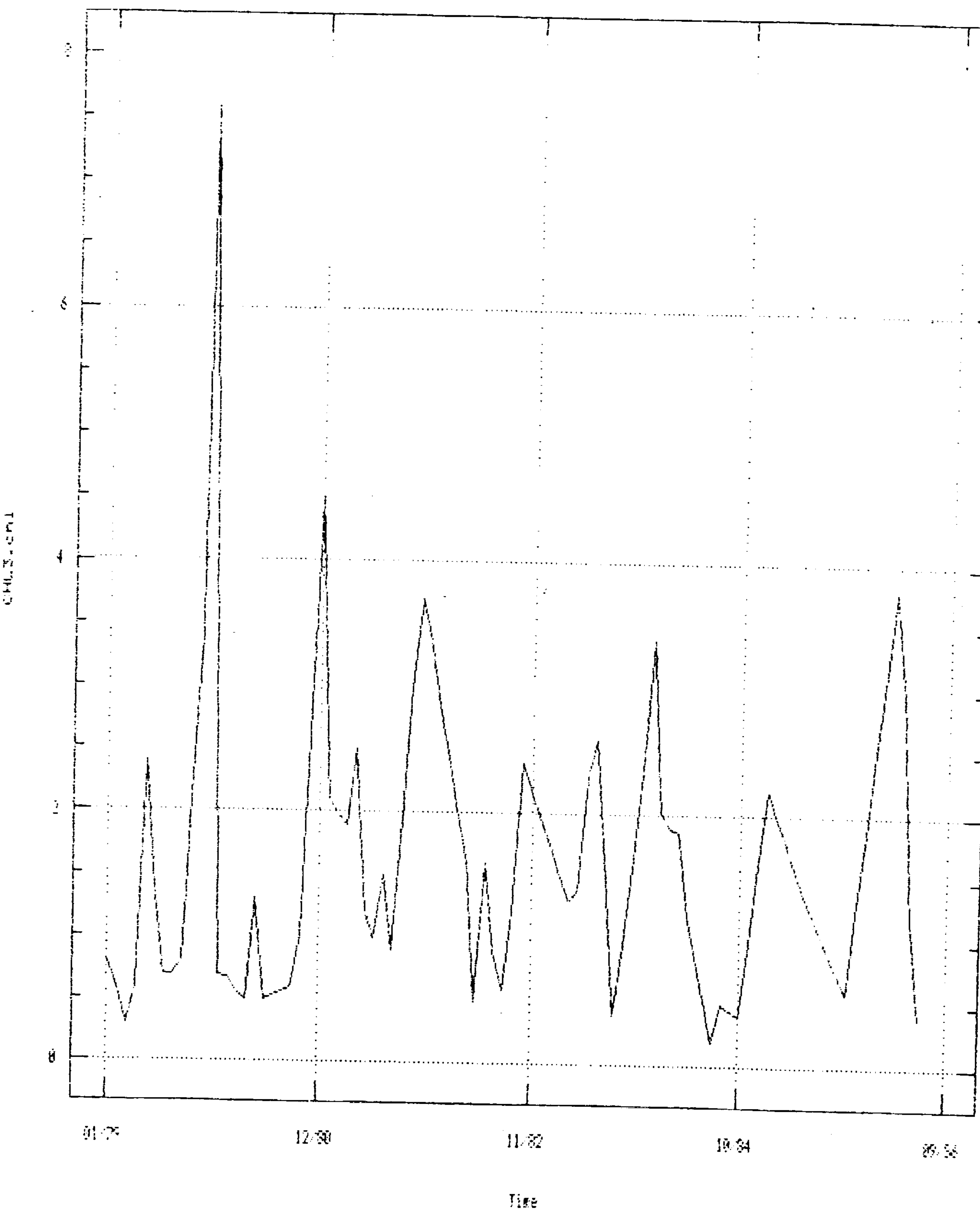

Time Sequence Plot

Box 4

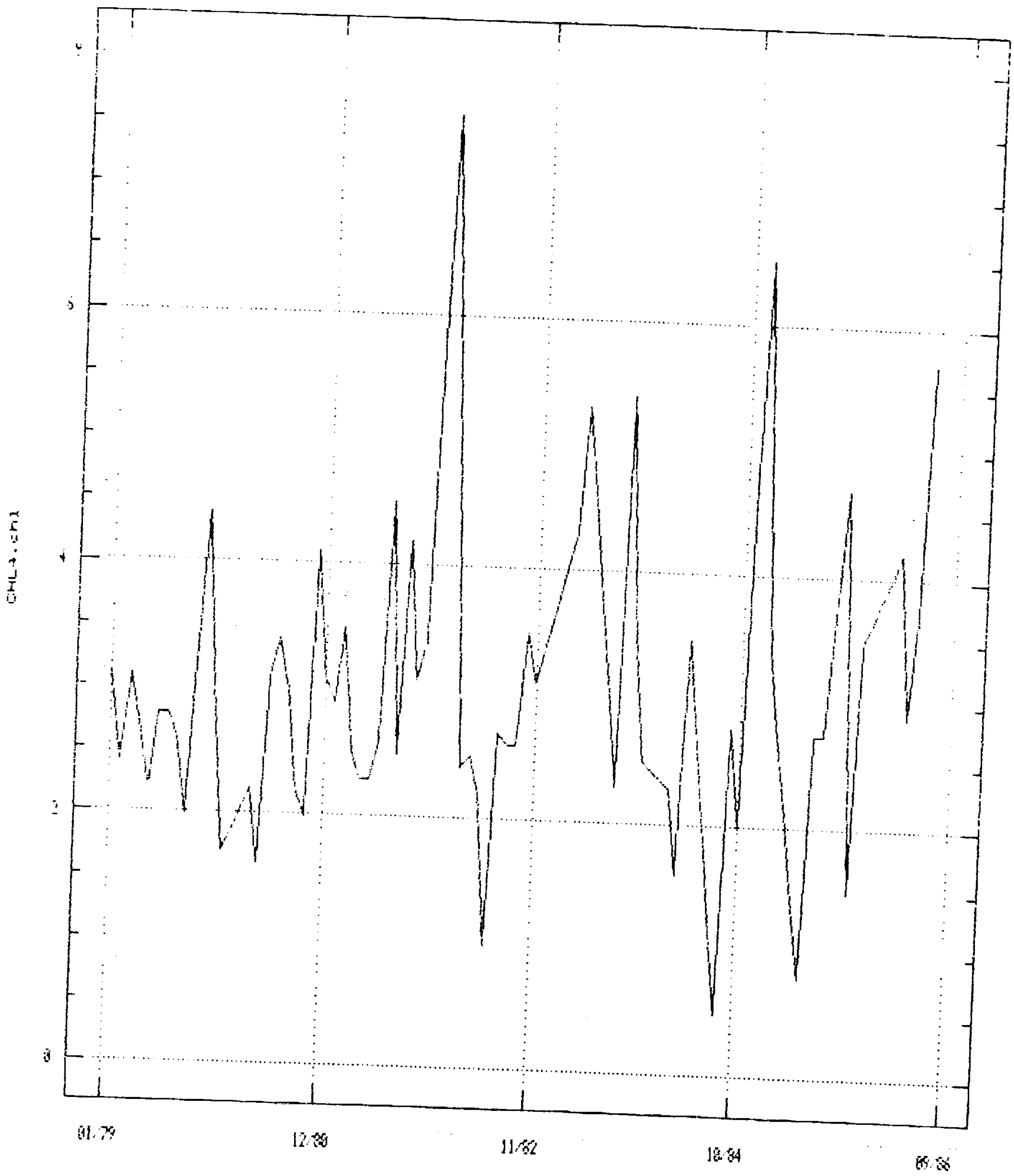

Time Sequence Plot

Box 5

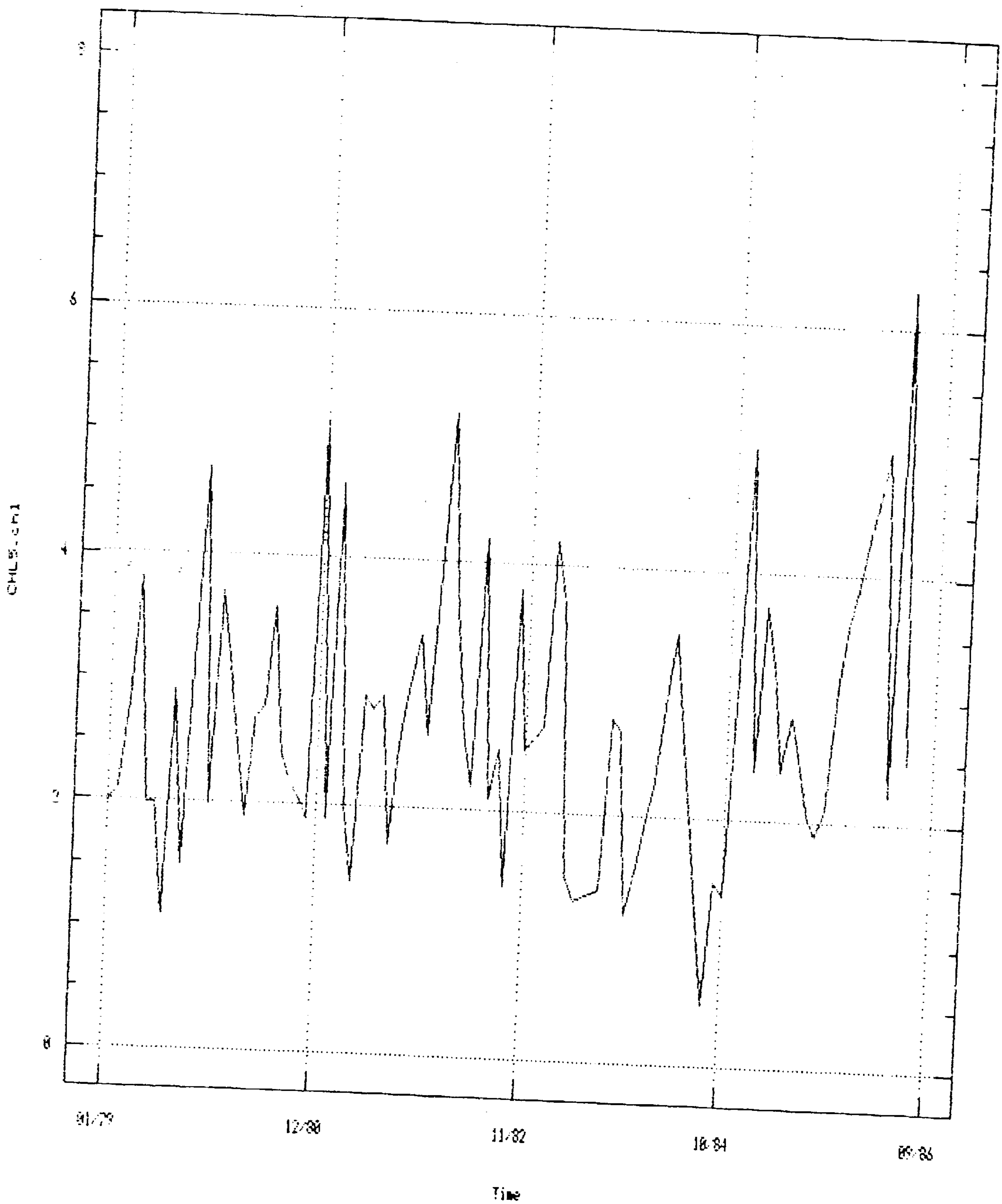

Portugal 1979-86: Box 6

Box 6

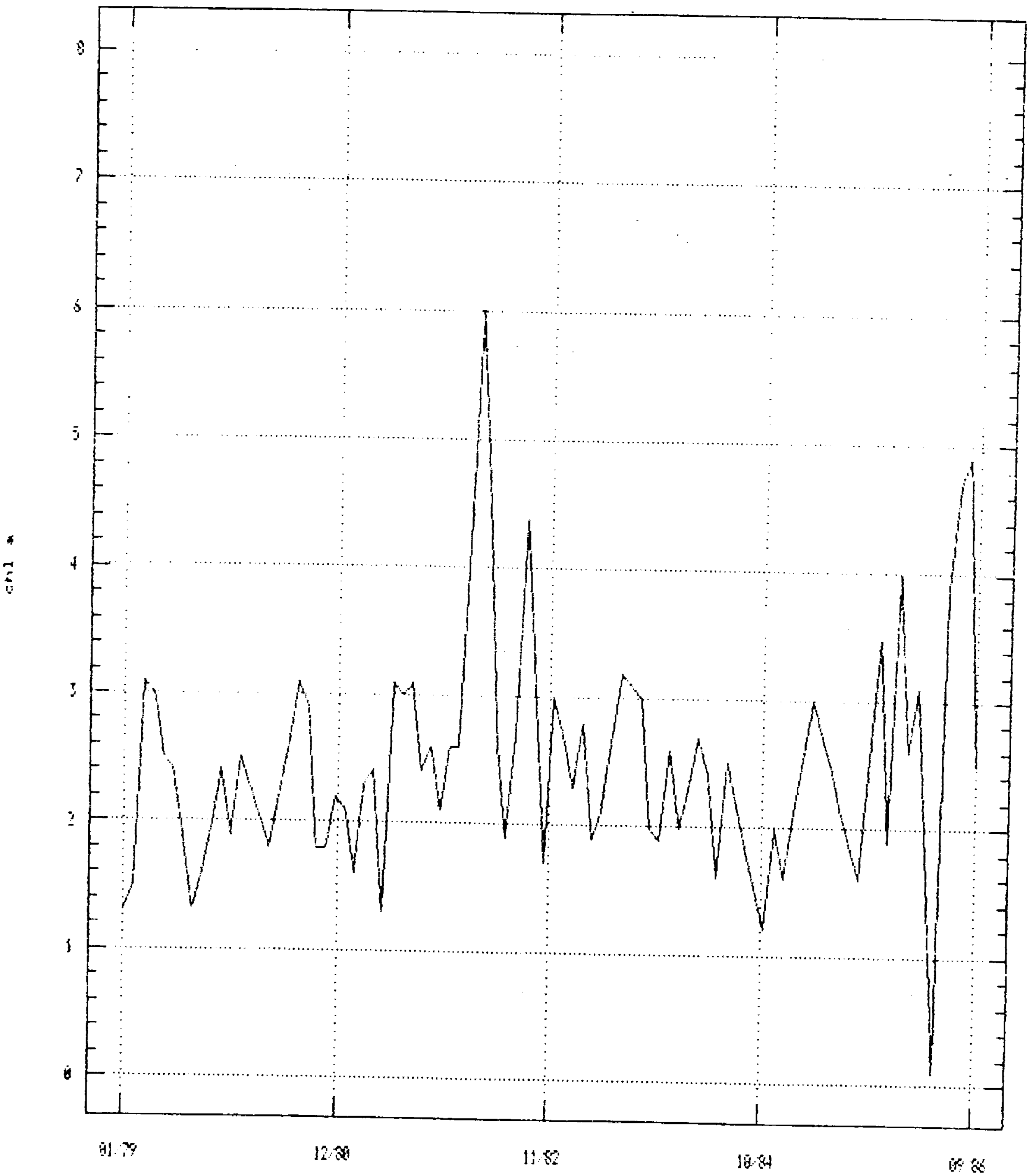

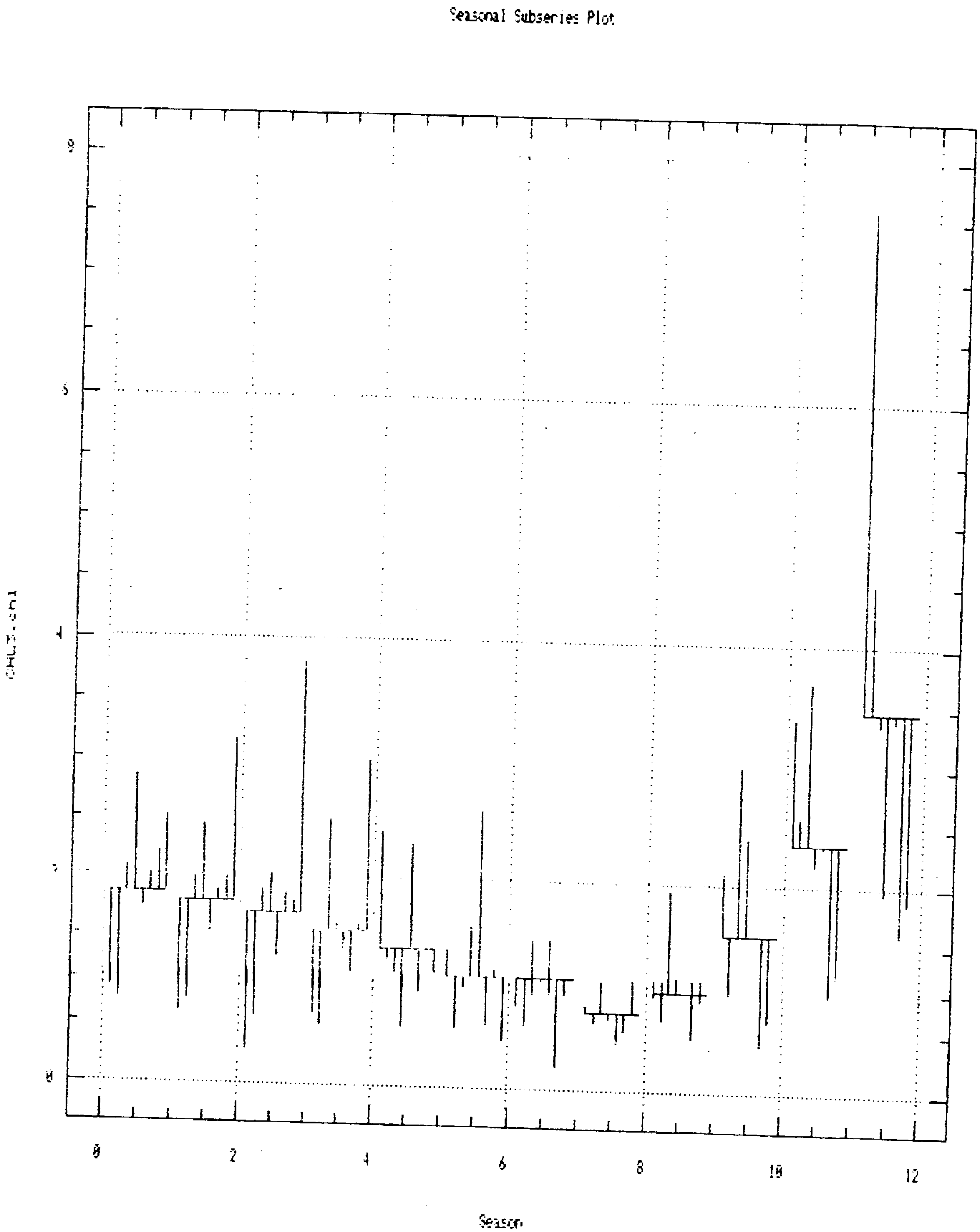

Box 3

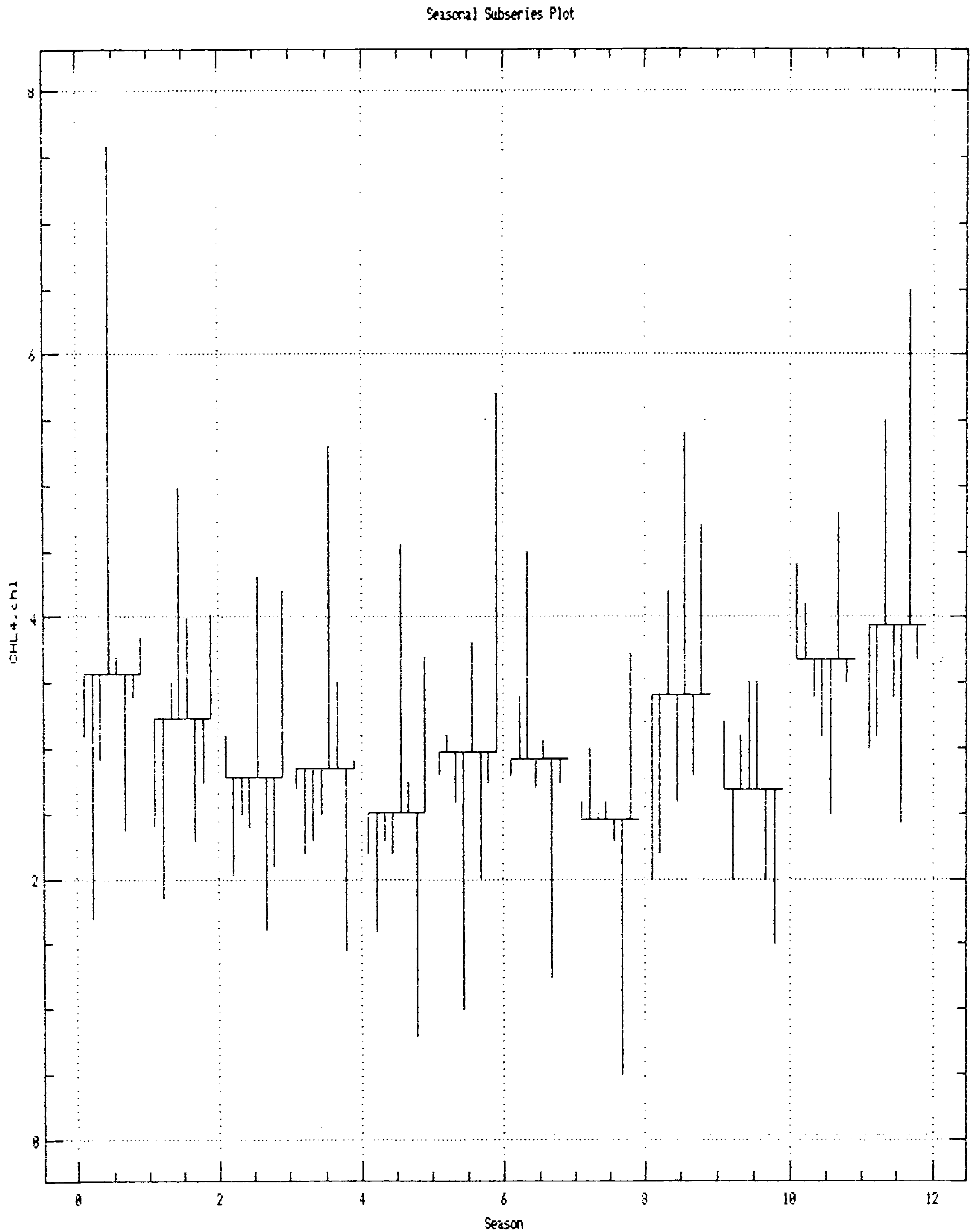

Box 4

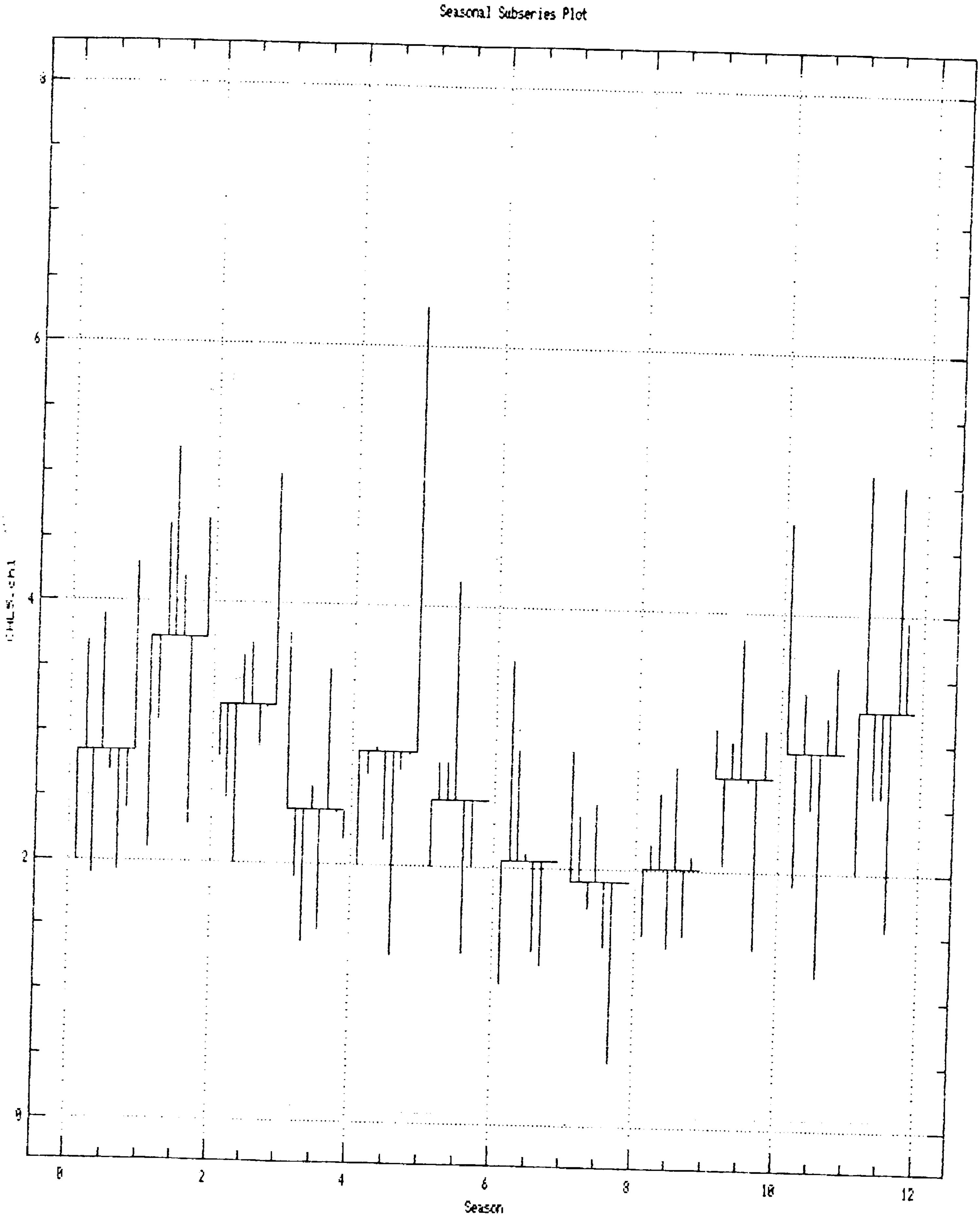

Box 5

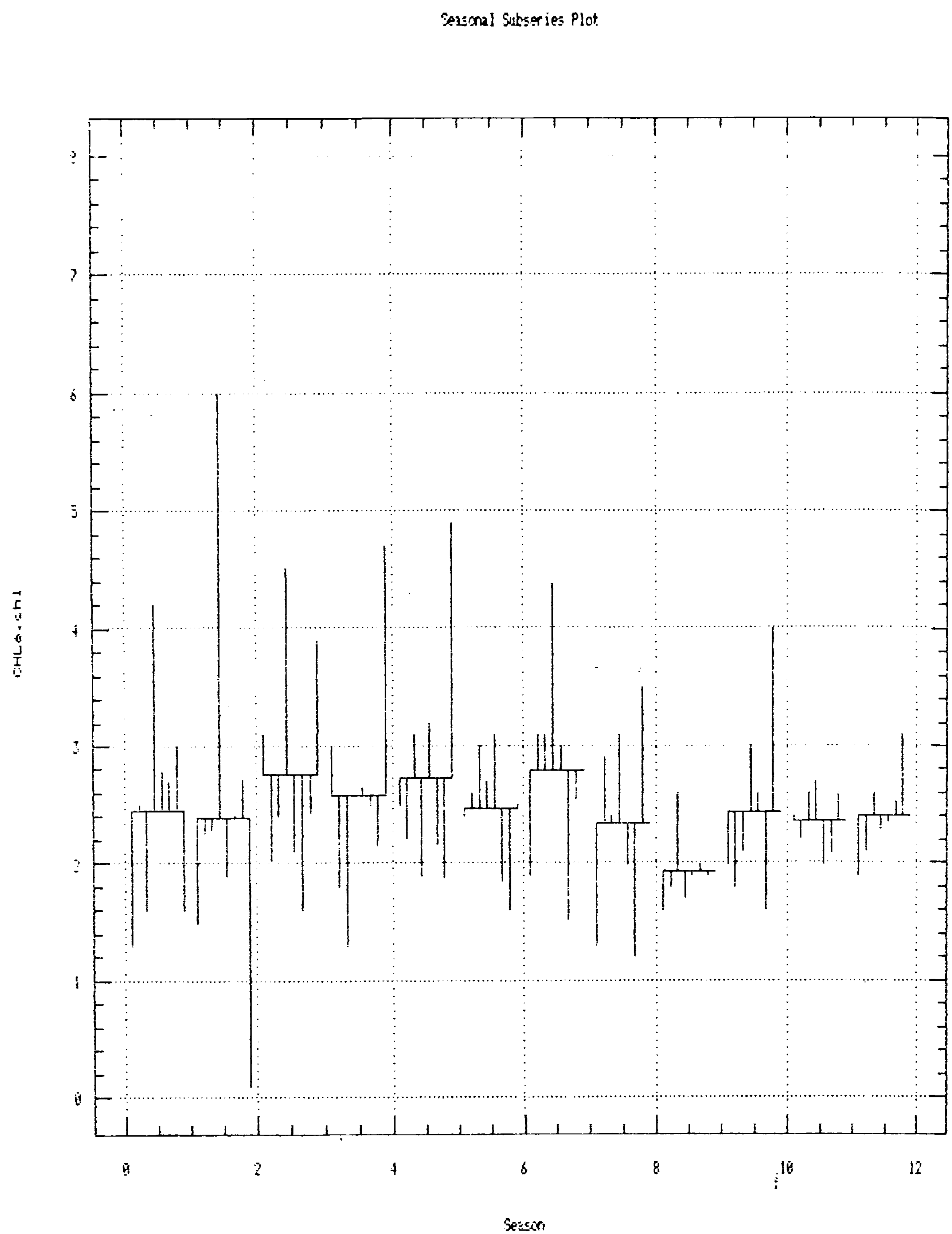

Box 6

Integrated periodogram for **Box 3**

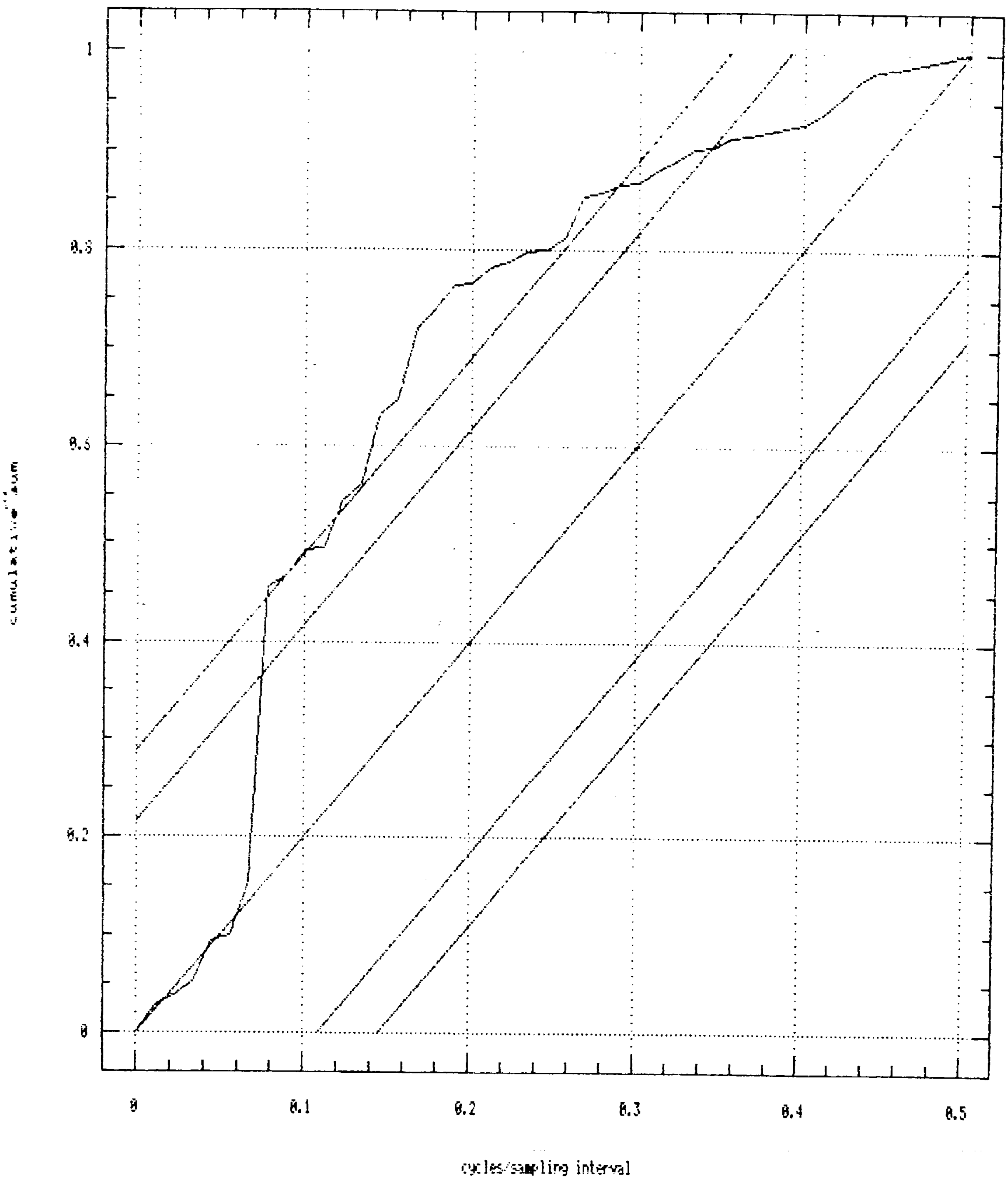

Integrated periodogram for Box 4

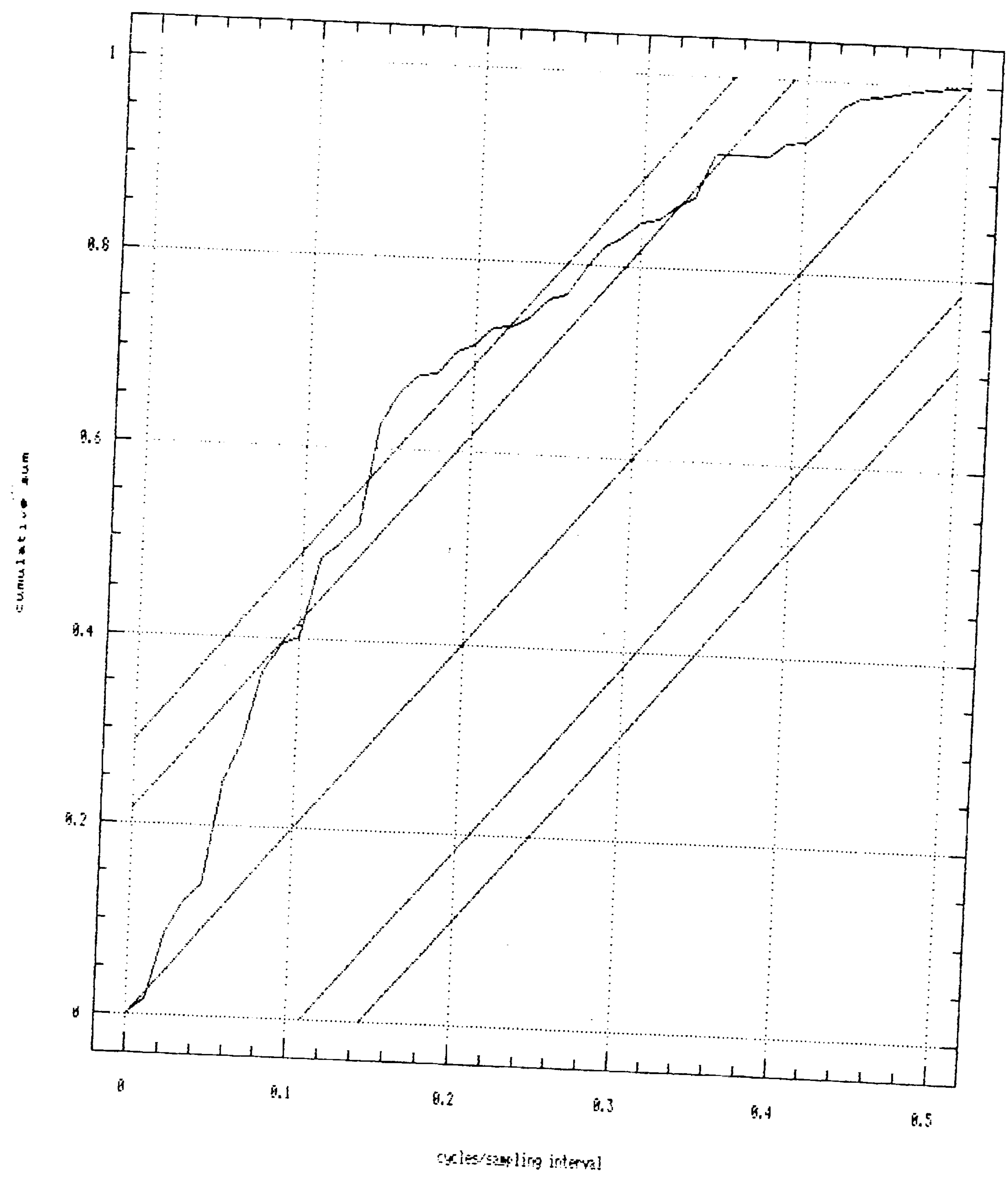

Integrated periodogram for Box 5

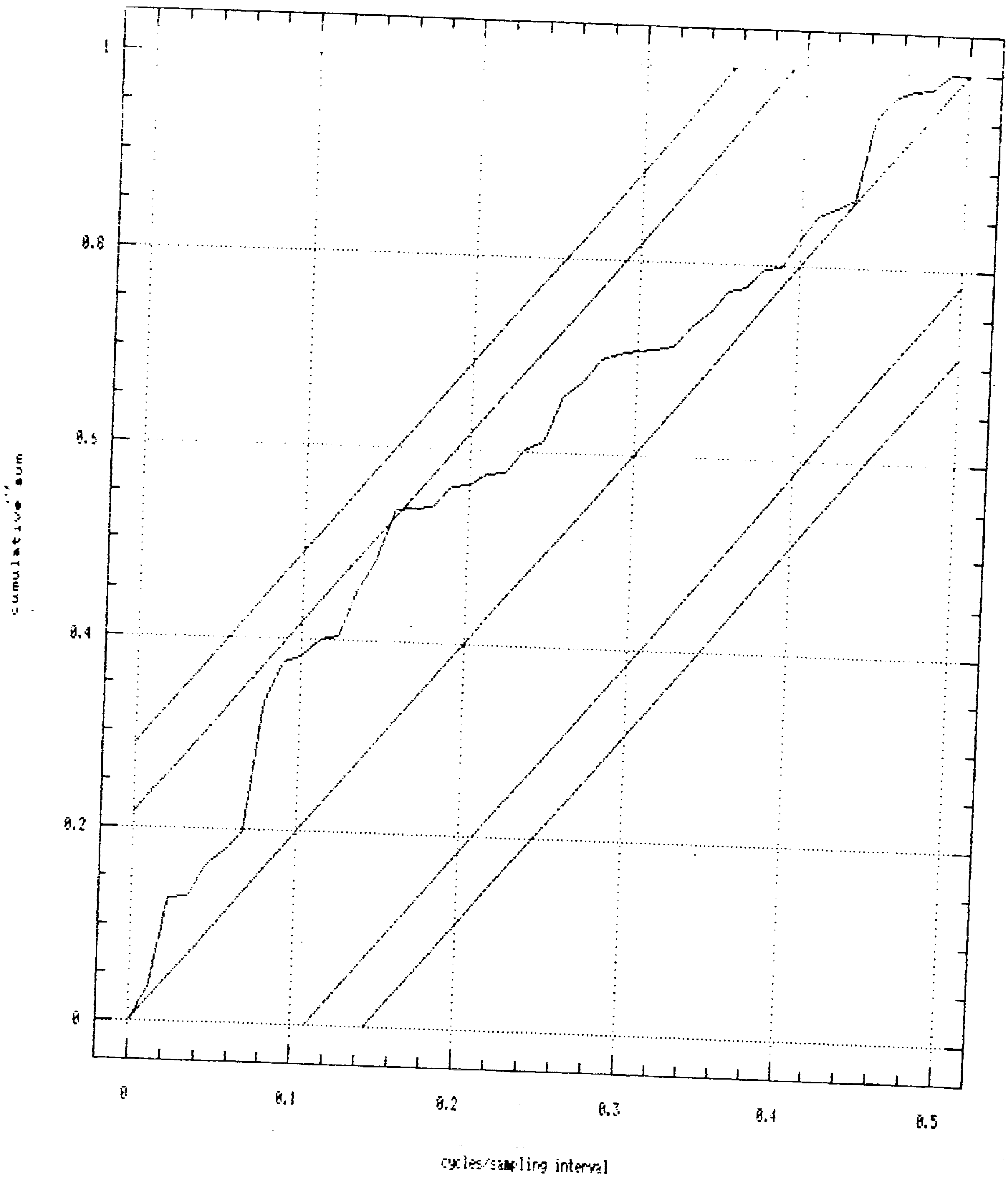

Integrated periodogram for **Box 6**:

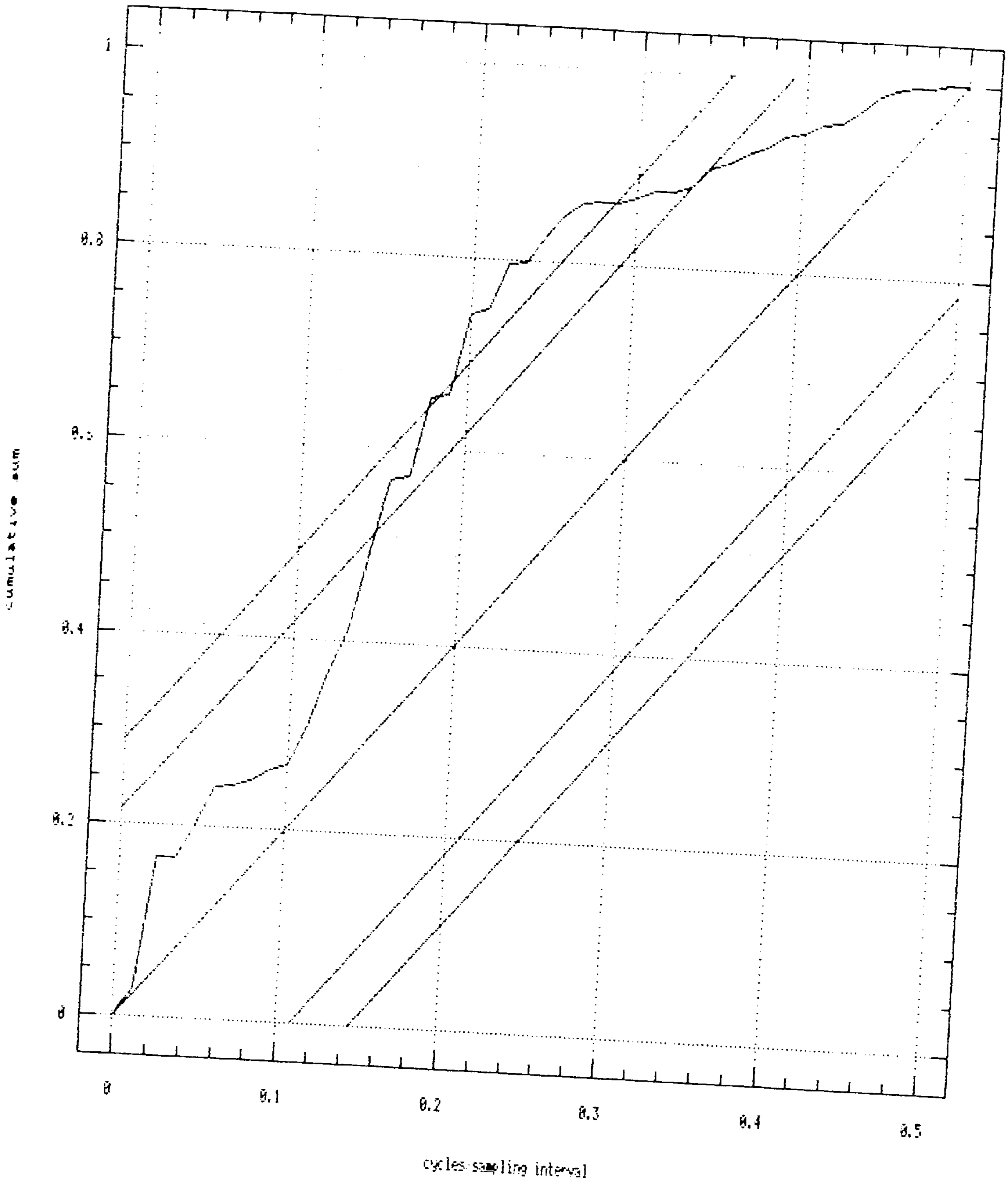

Estimated Cross-Correlations

Box 3 vs Box 4

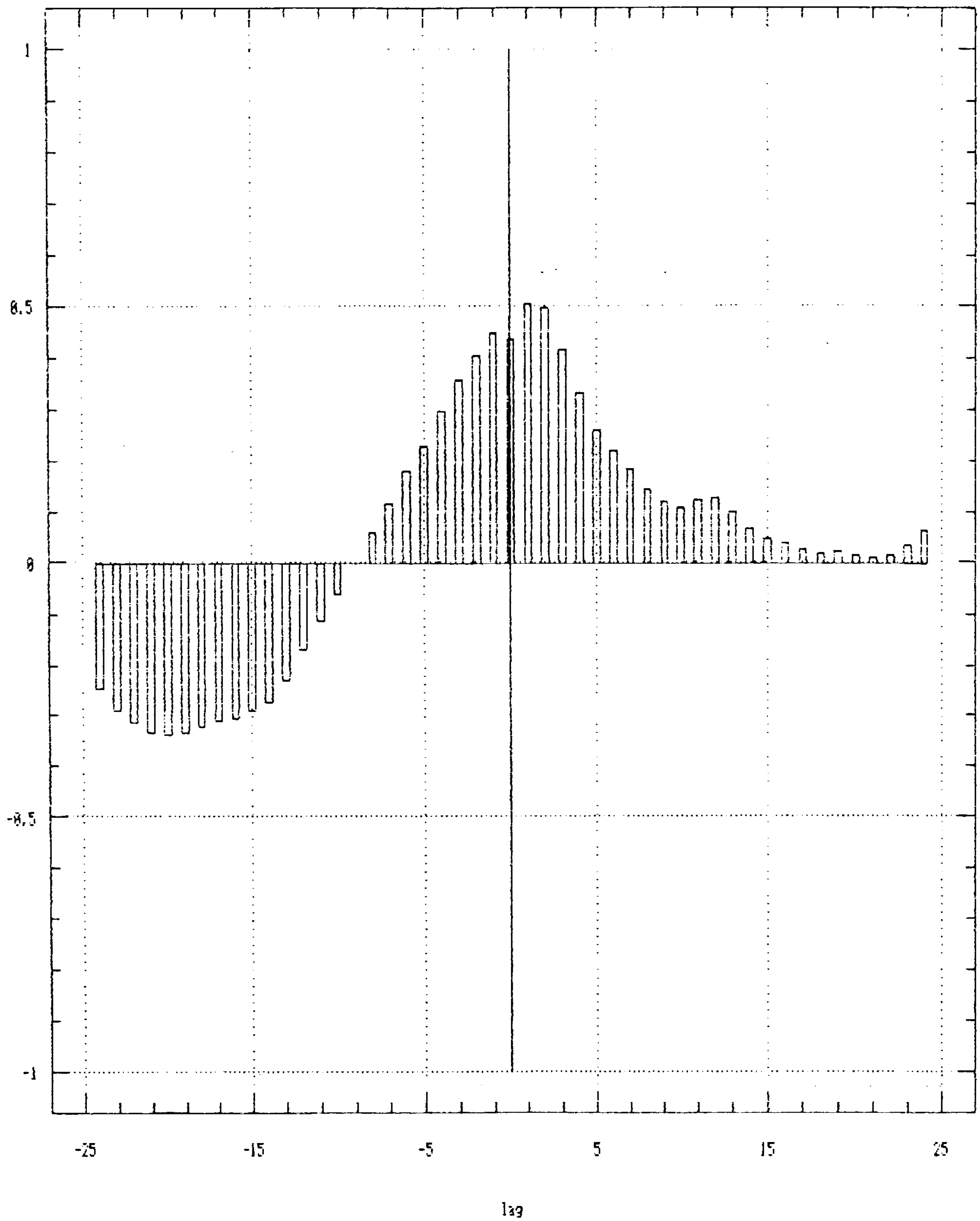

Estimated Cross-Correlations

Box 3 vs Box 5

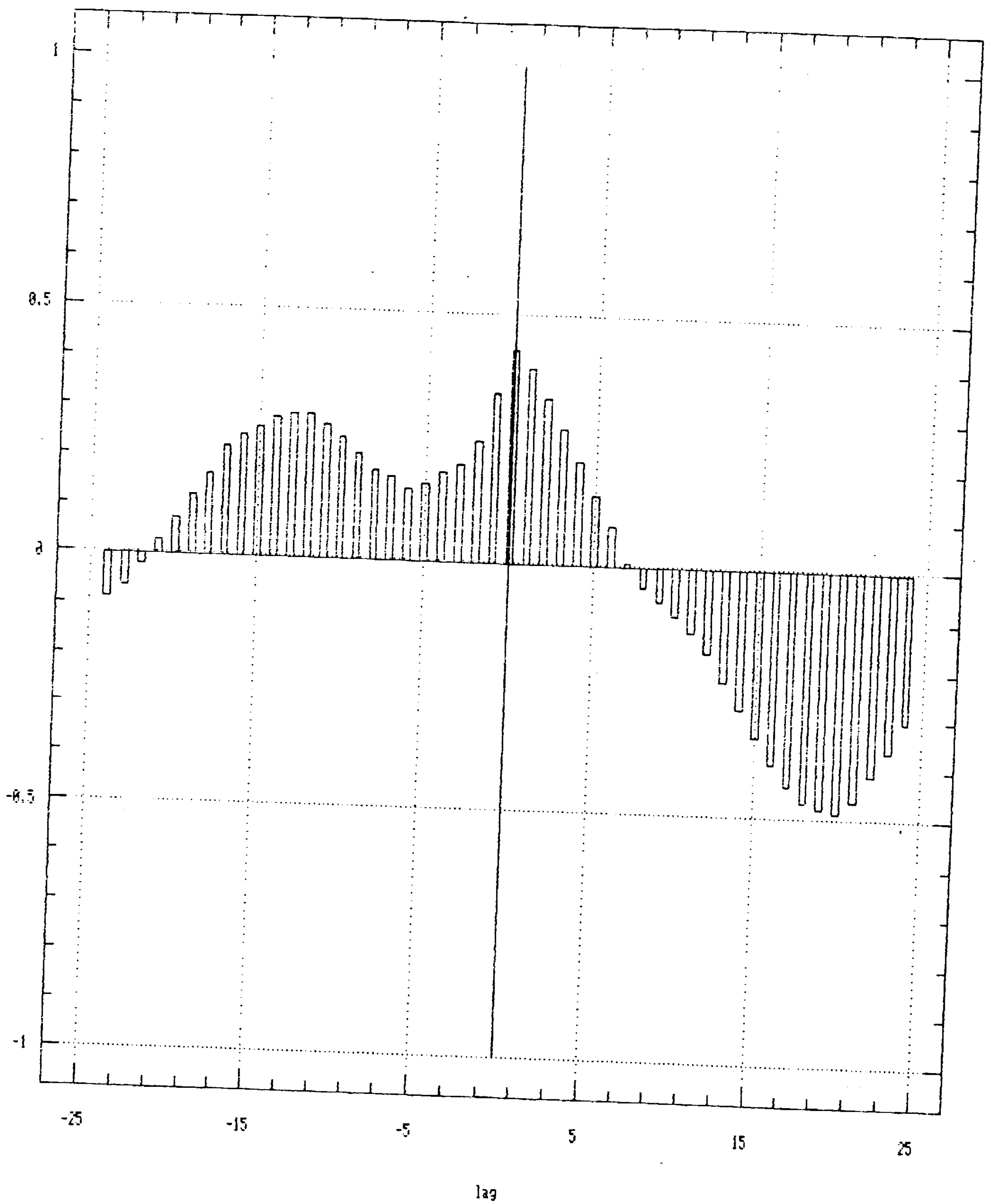

Estimated Cross-Correlations

Box 3 vs Box 6

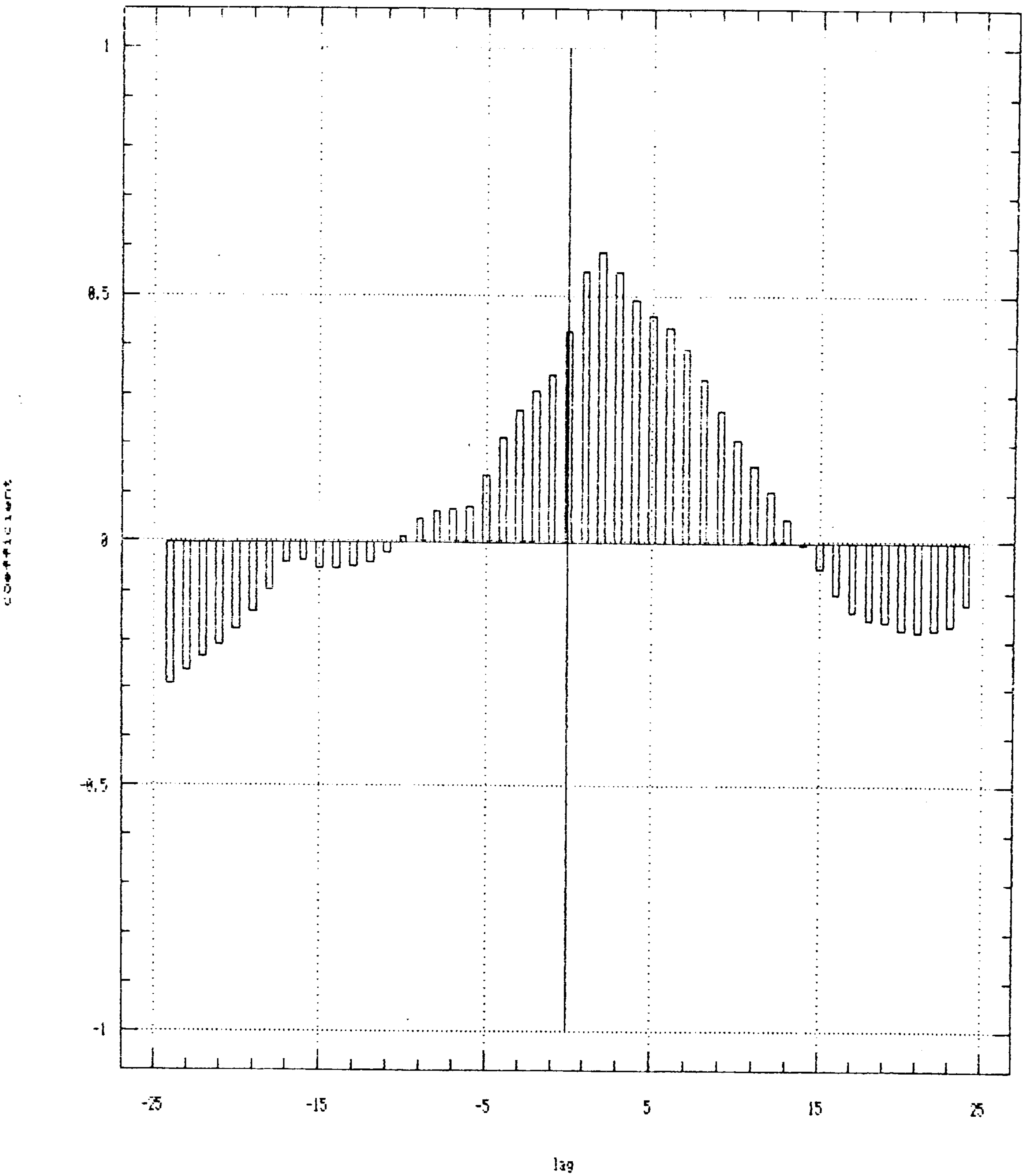

Estimated Cross-Correlations

Box 4 vs Box 3

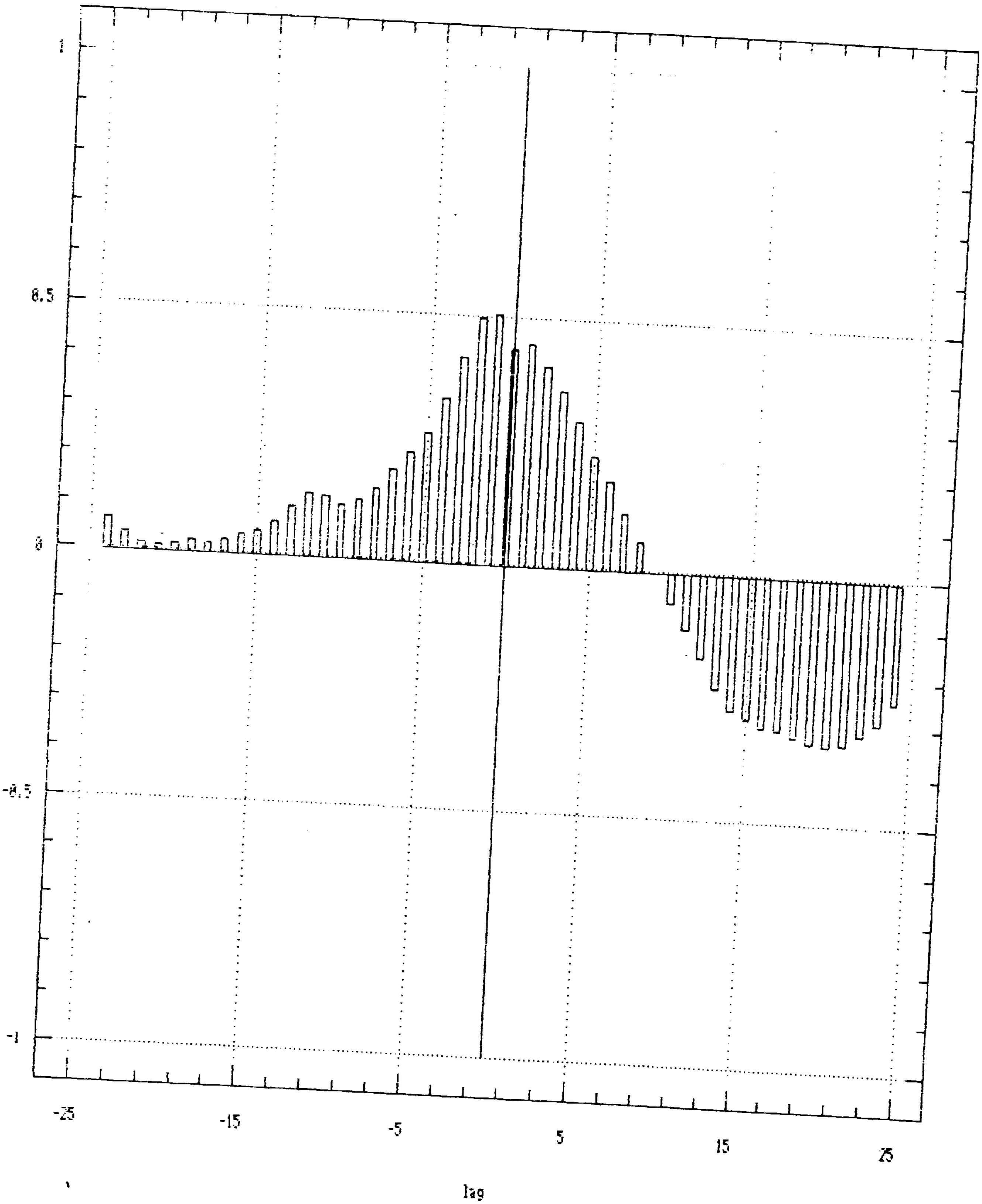

Estimated Cross-Correlations

Box 4 vs Box 5

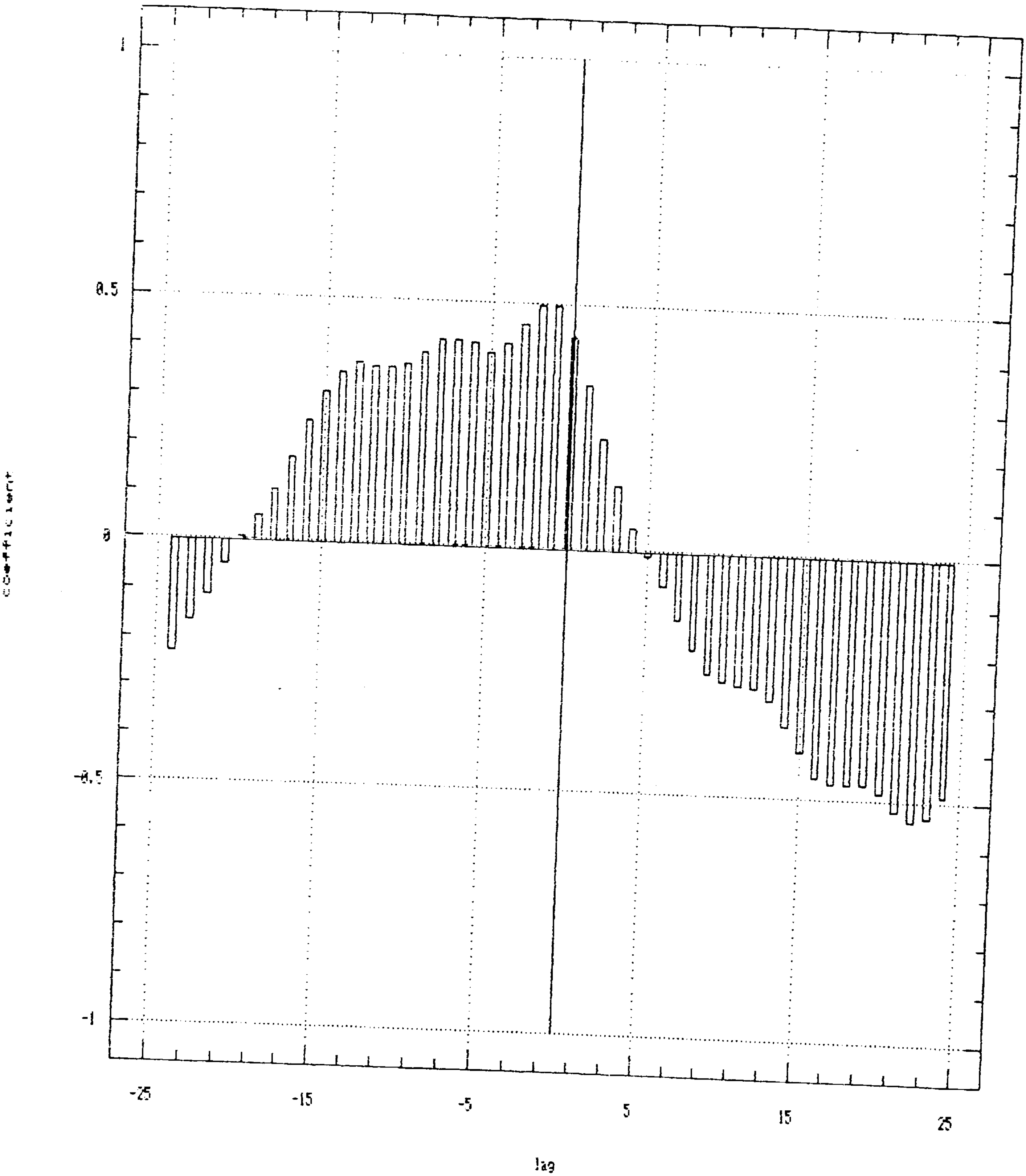

Estimated Cross-Correlations

Box 4 vs Box 6

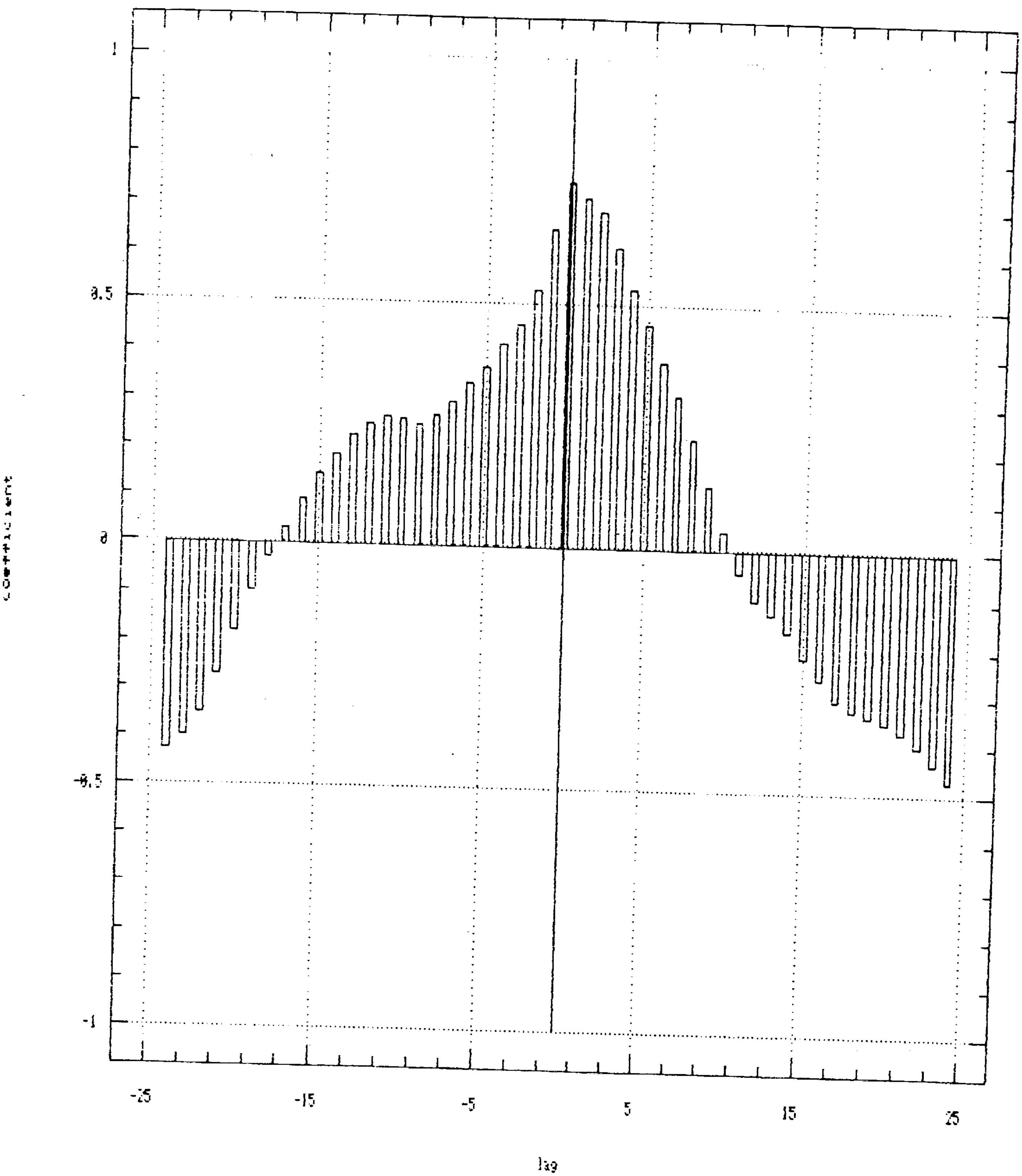

Estimated Cross-Correlations

Box 5 vs Box 3

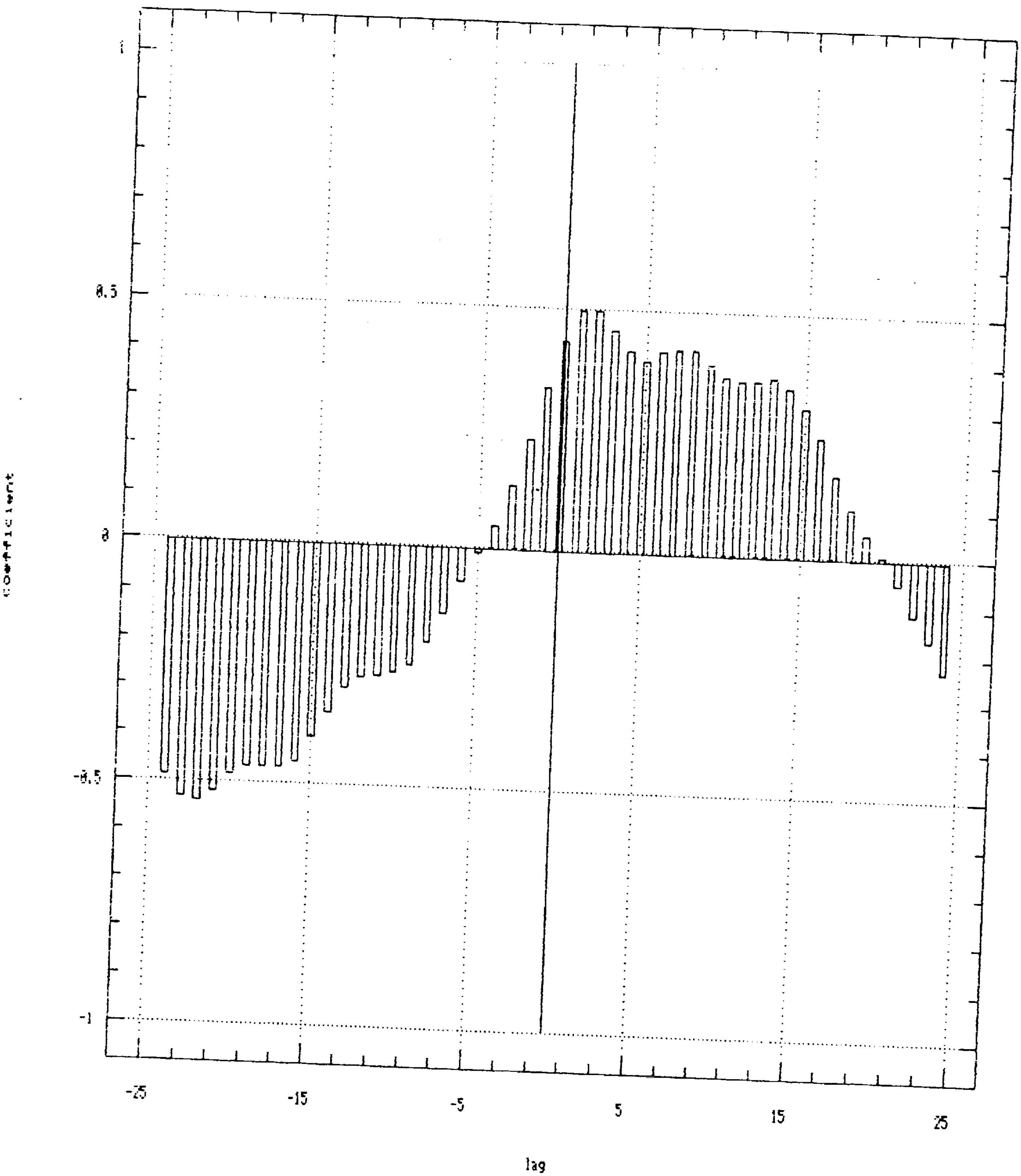

Estimated Cross-Correlations

Box 5 vs Box 6

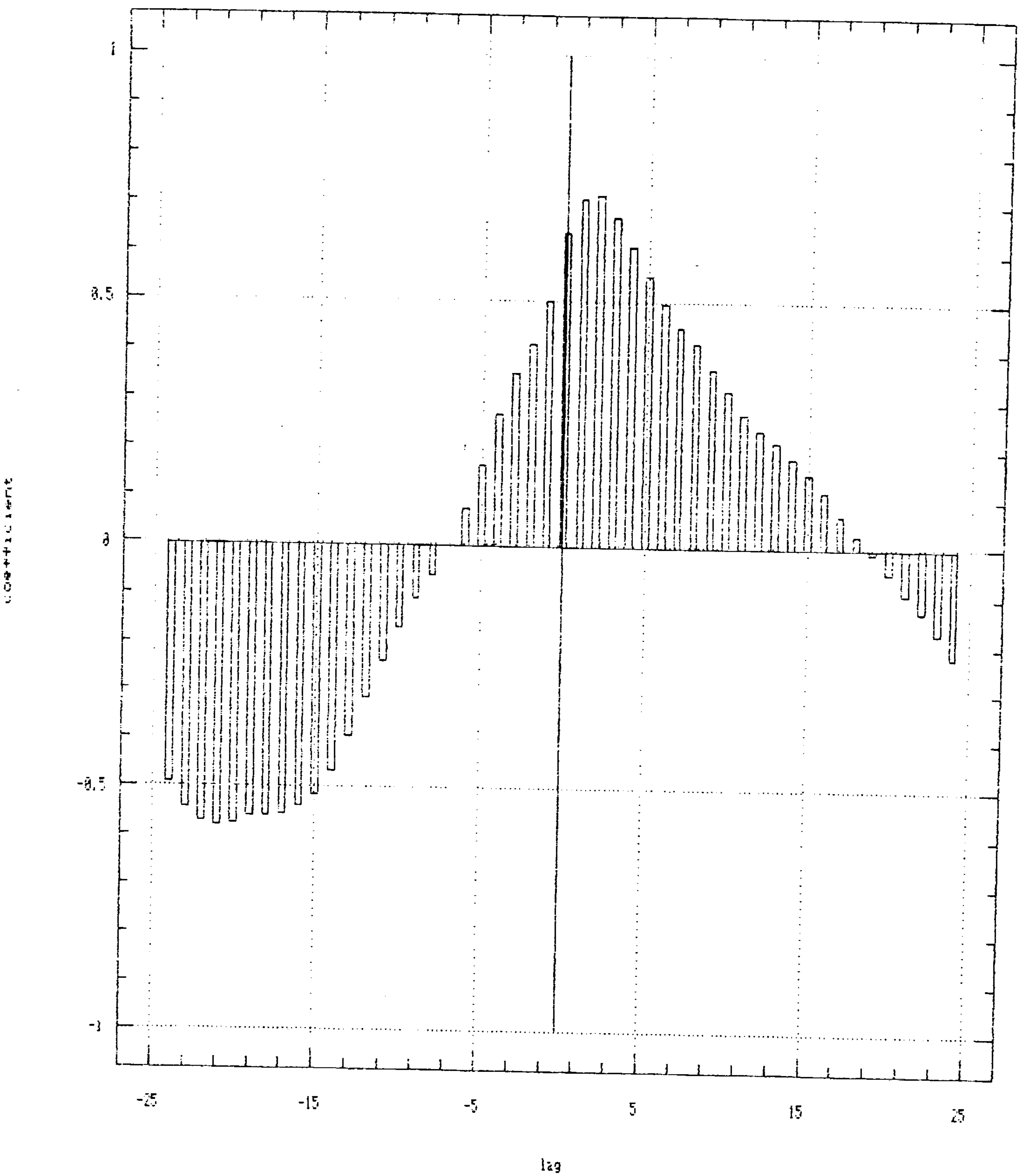

Estimated Cross-Correlations

Box 6 vs Box 3

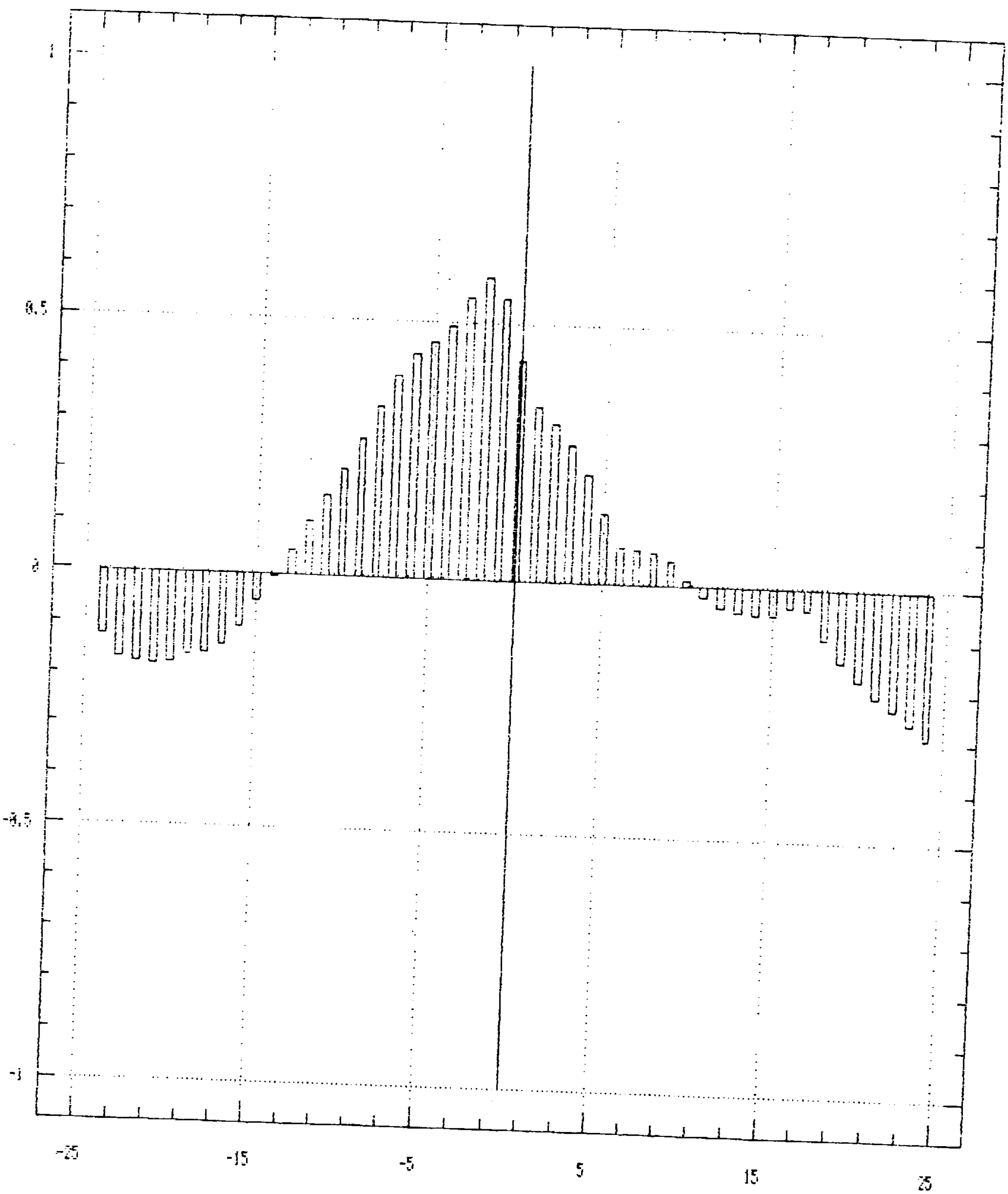

Estimated Cross-Correlations

Box 6 vs Box 4

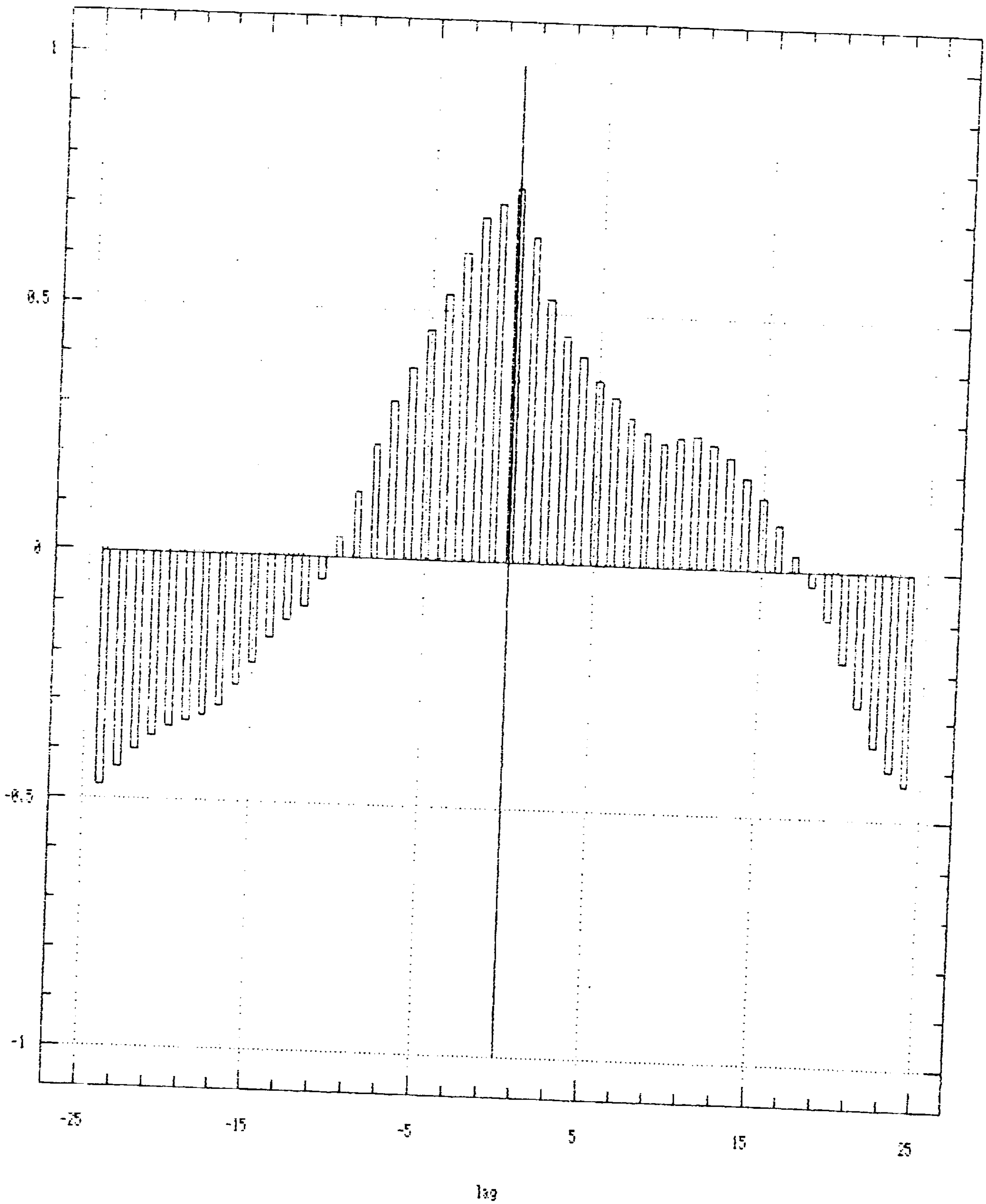

Estimated Cross-Correlations

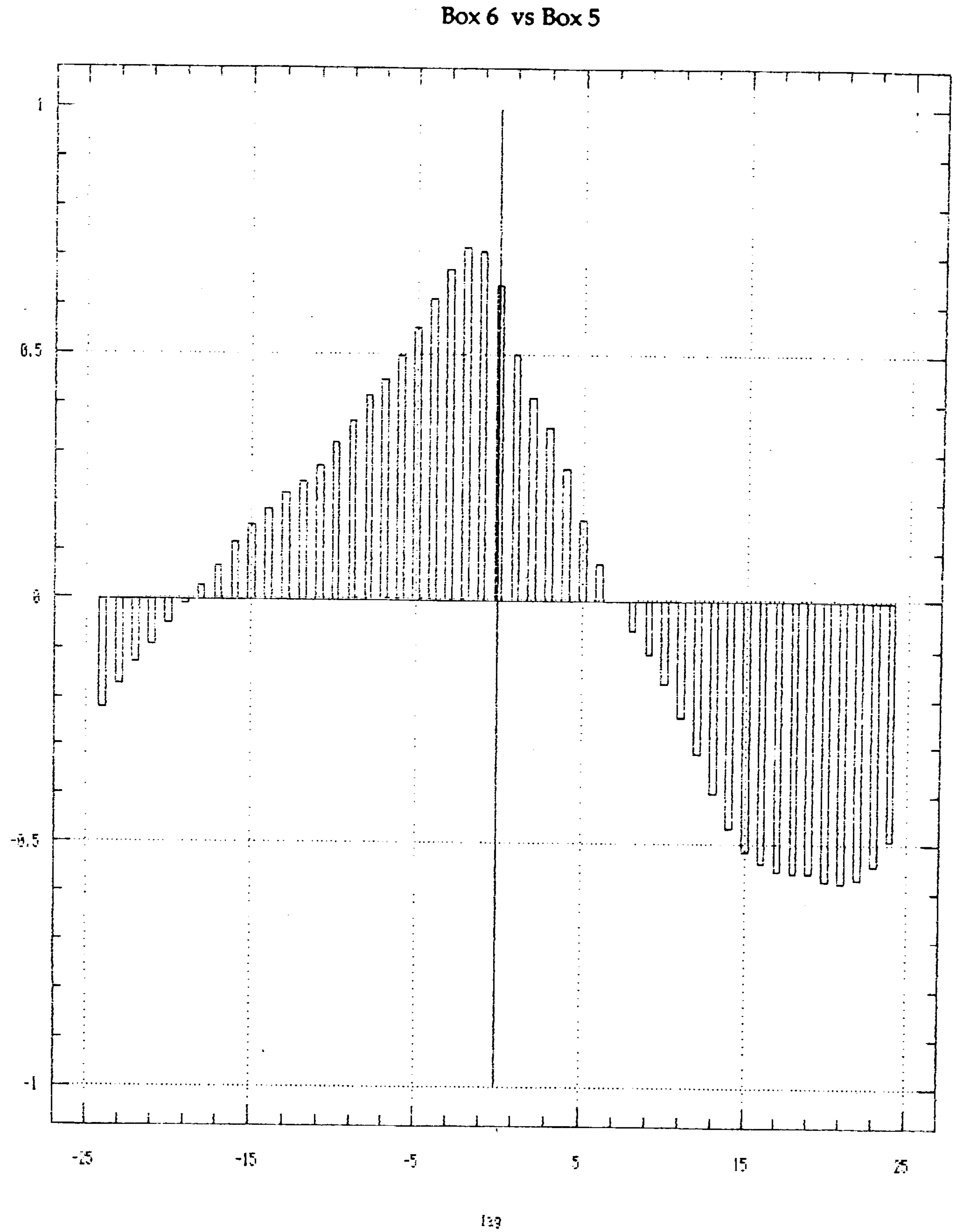

Estimated Cross-Correlations

NS 3 vs Box 3

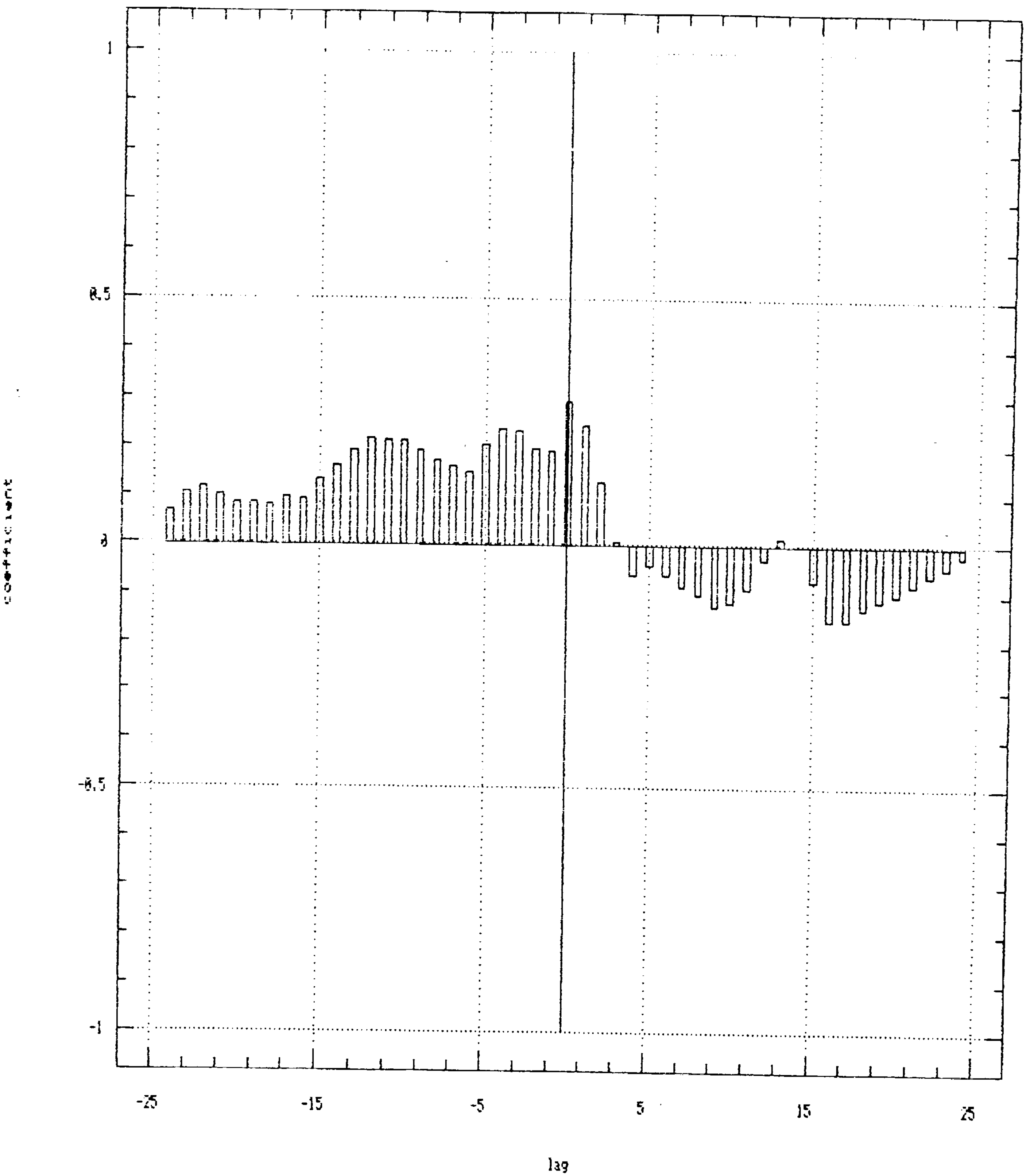

Estimated Cross-Correlations

NS 5 vs Box 5

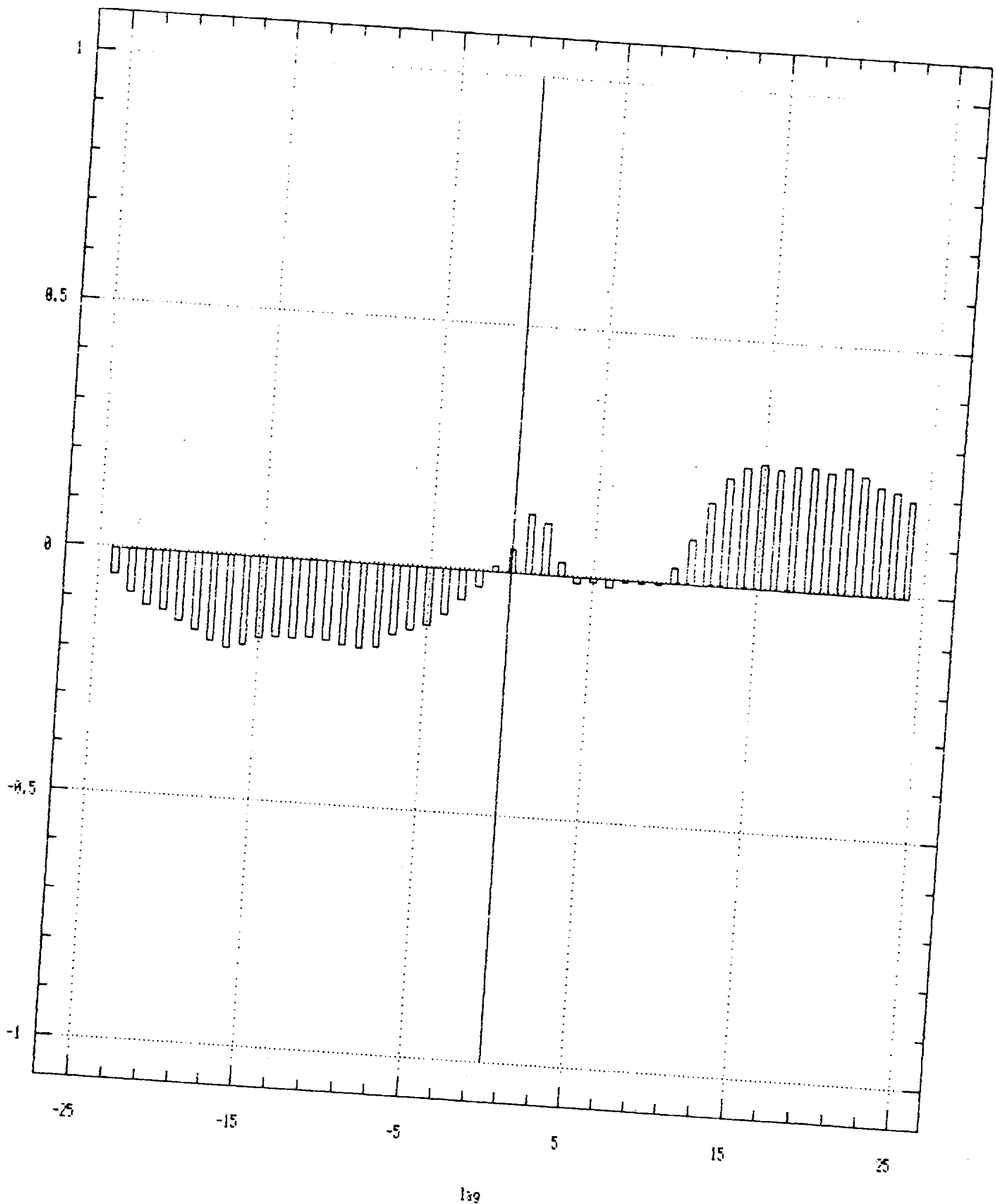

Estimated Cross-Correlations

NS 4 vs Box 4

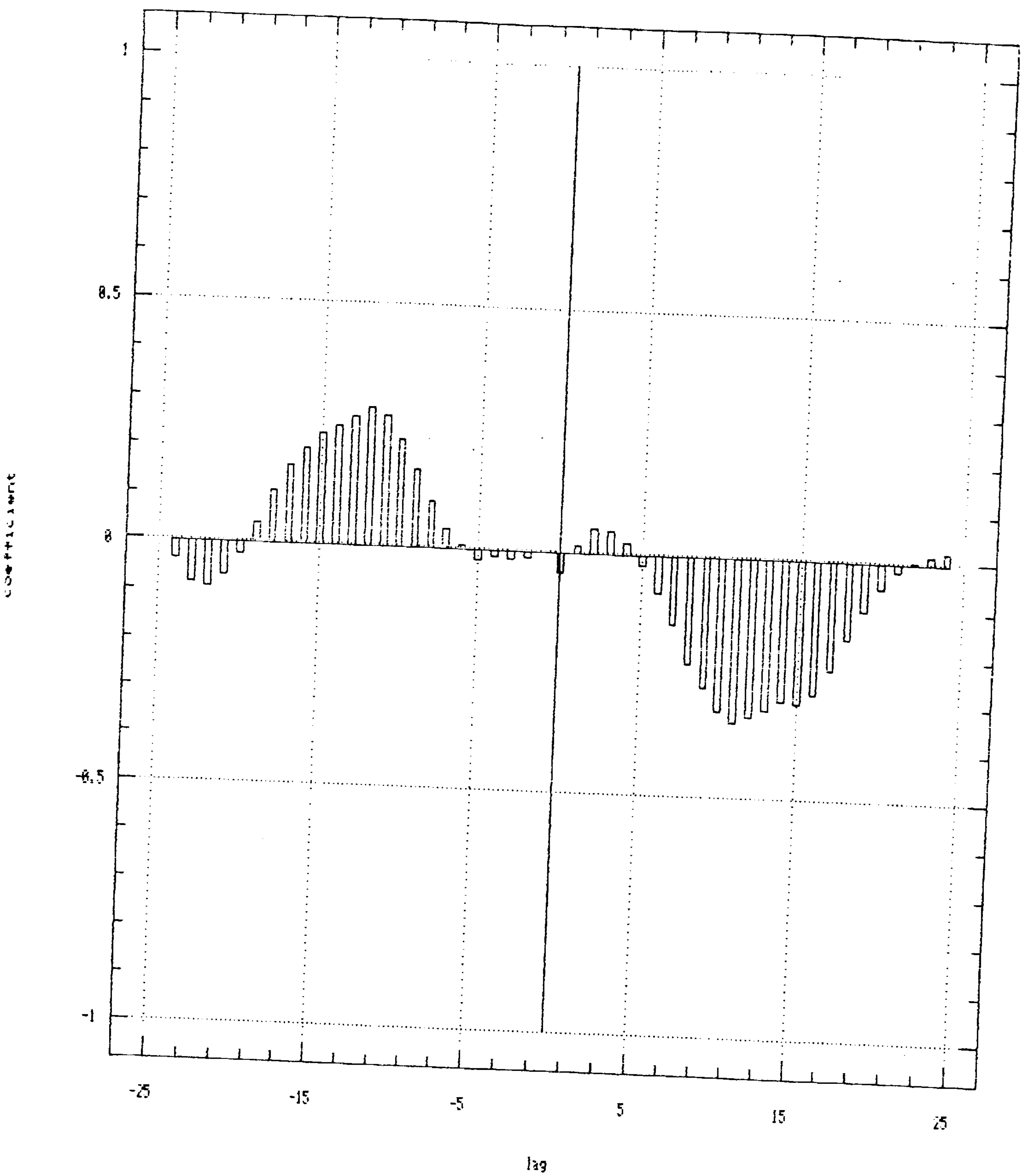

Estimated Cross-Correlations

NS 6 vs Box 6

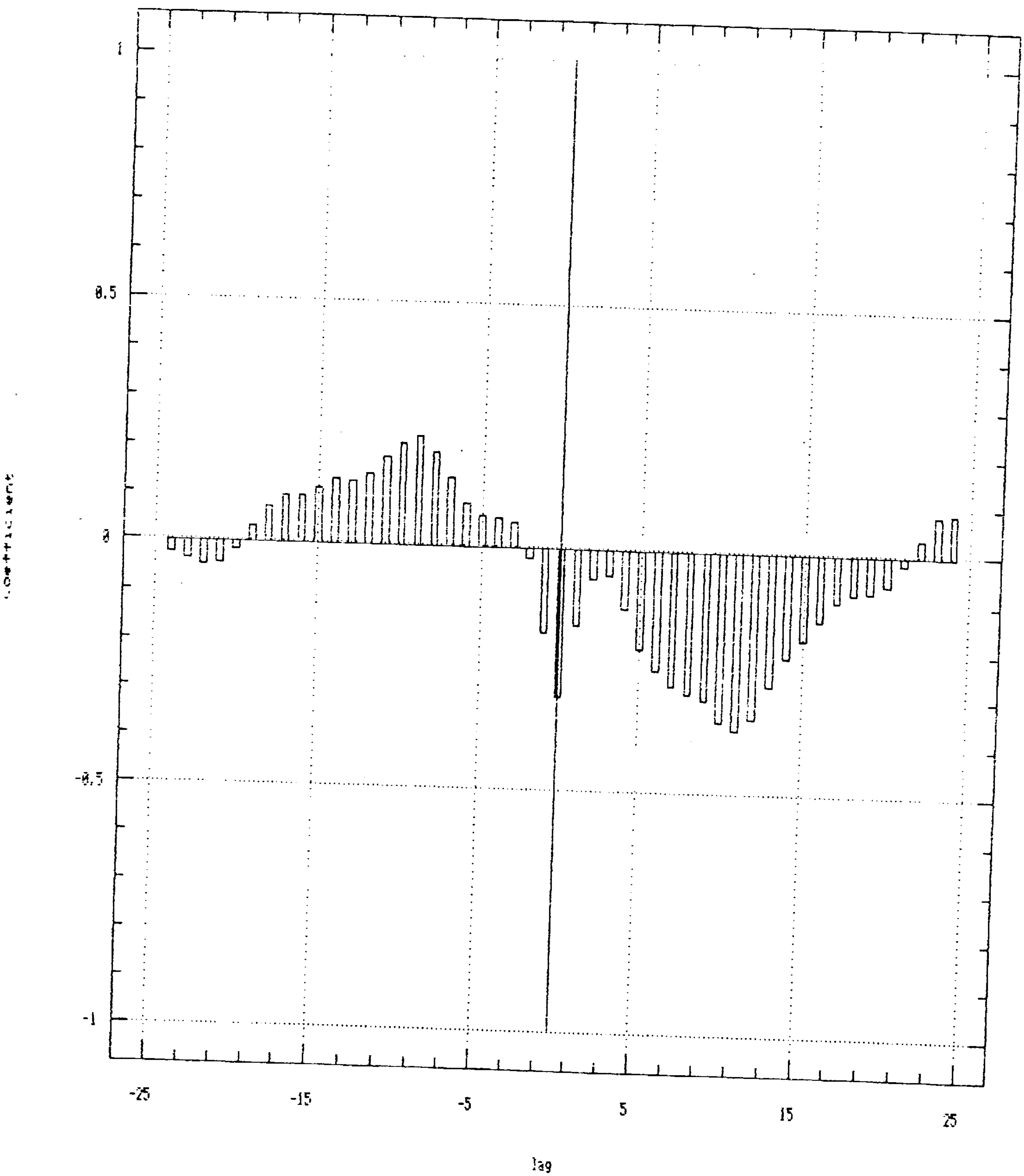

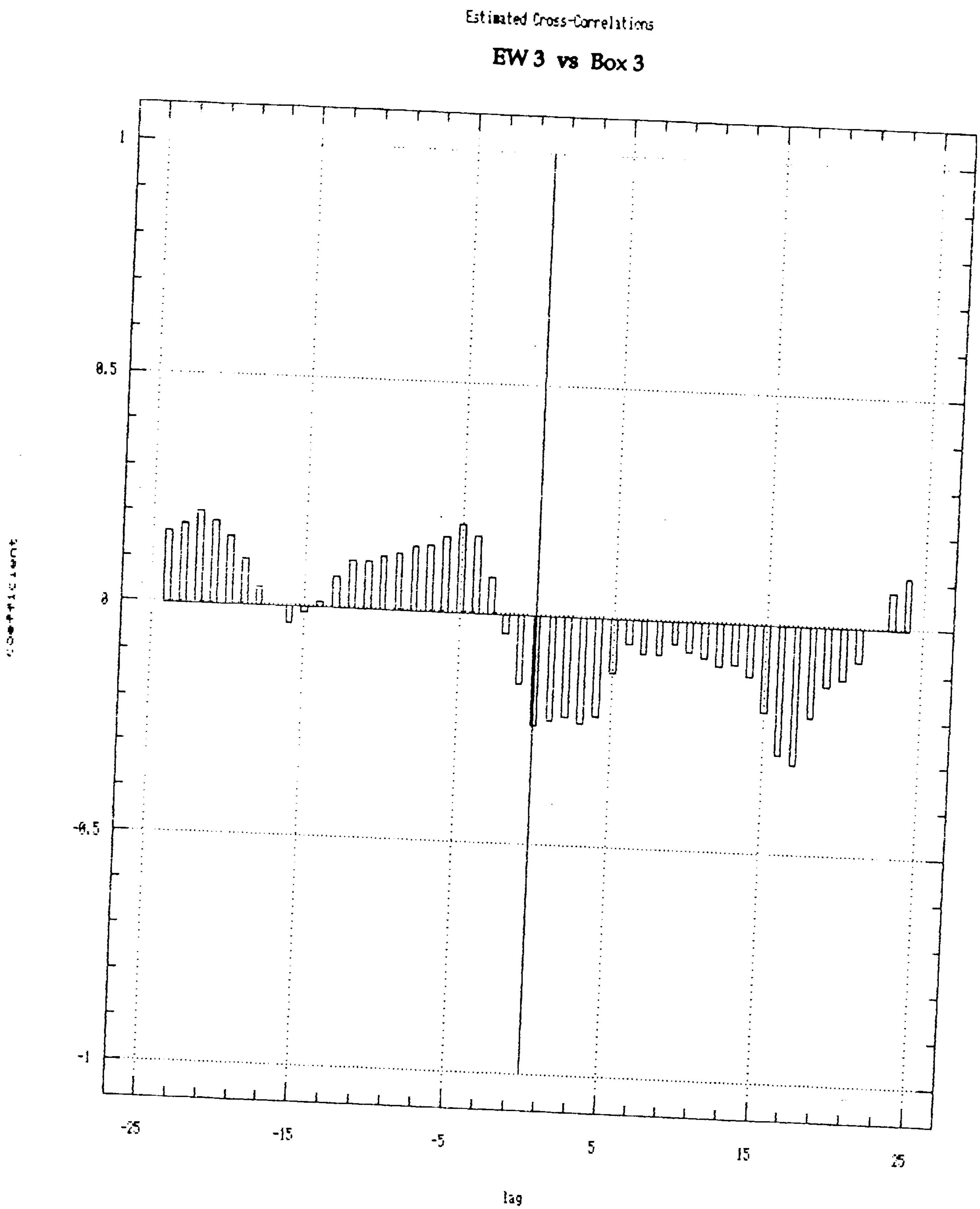

Estimated Cross-Correlations
EW 3 vs Box 3
1
0.5
0
-0.5
-1
-25
-15
-5
5
15
25
lag
coefficient

Estimated Cross-Correlations

EW 4 vs Box 4

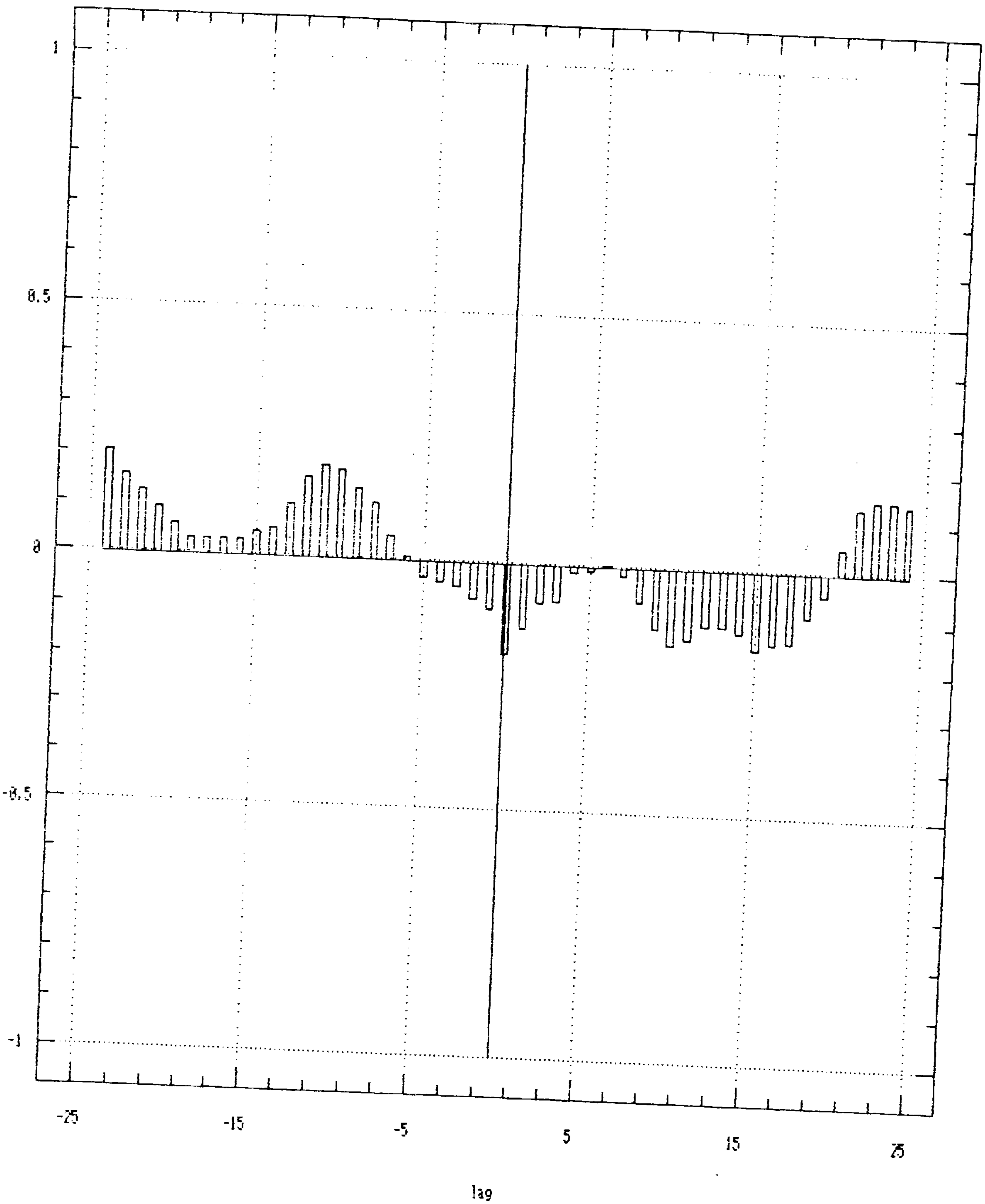

Estimated Cross-Correlations

EW 5 vs Box 5

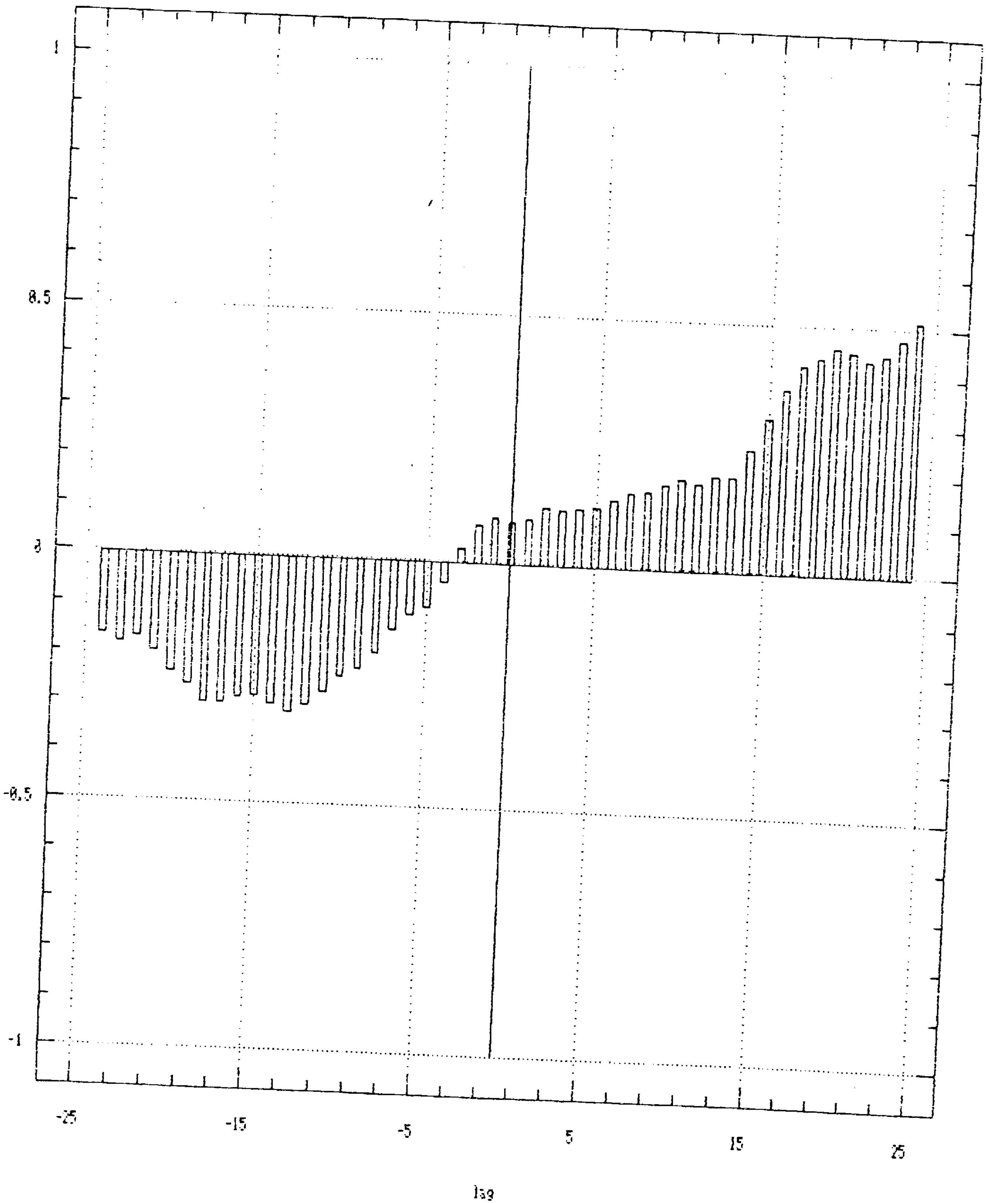

Estimated Cross-Correlations

EW 6 vs Box 6